Available online at www.sciencedirect.com
ScienceDirect
Finite Elements in Analysis and Design 43 (2007) 425–443
FINITE ELEMENTS IN ANALYSIS AND DESIGN
www.elsevier.com/locate/finel

Non-linear geometrically exact assumed stress–strain four-node solid-shell element with high coarse-mesh accuracy

G.M. Kulikov*, S.V. Plotnikova

Department of Applied Mathematics and Mechanics, Tambov State Technical University, Sovetskaya Street 106, Tambov 392000, Russia

Received 20 September 2005; received in revised form 25 October 2006; accepted 30 November 2006
Available online 25 January 2007

Abstract

This paper presents a family of geometrically exact assumed stress–strain four-node solid-shell elements with six displacement degrees of freedom per node based on the finite rotation first-order multilayered shell theory. The proposed formulation is based on the new objective non-linear strain–displacement relationships, which are invariant under arbitrarily large rigid-body motions. To improve a non-linear shell response, the modified assumed natural strain method is applied. This enhanced non-linear solid-shell element formulation allows using coarser meshes. To avoid shear and membrane locking and have no spurious zero energy modes, the assumed strain and stress resultant fields are invoked. In order to circumvent thickness locking, the ad hoc modified laminate constitutive stiffness matrix corresponding to the generalized plane stress condition is employed. The fundamental unknowns consist of six displacements and nine strains of the face and middle surfaces of the shell, and nine conjugate stress resultants. For the analytical description of surface geometry, an effective numerical algorithm of smoothing the data by cubic spline functions developed by the first author as early as 1981 is used. To demonstrate the efficiency and accuracy of the developed non-linear geometrically exact solid-shell element and to compare its performance with isoparametric elements, extensive numerical studies are presented.

Keywords: Finite rotation; Four-node solid-shell element; Assumed stress–strain formulation; First-order shell theory; Spline surface

1. Introduction

In recent years, a considerable work has been carried out on three-dimensional (3D) continuum-based non-linear finite elements that can handle thin shell analyses satisfactorily. These elements are typically defined by two layers of nodes at the bottom and top surfaces of the shell with three displacement degrees of freedom per node and known as *isoparametric* solid-shell elements [1–10]. In the isoparametric solid-shell element formulation, initial and deformed geometry are equally interpolated allowing one to describe rigid-body motions precisely. The development of solid-shell elements is not straightforward [11]. In order to overcome element deficiencies such as shear, membrane, trapezoidal and thickness locking, advanced finite element techniques including assumed natural strain (ANS), hybrid strain, enhanced assumed strain and hybrid stress methods have been applied. Still, the isoparametric solid-shell element formulation is computationally inefficient because stresses and strains are analyzed in the global and local orthogonal Cartesian coordinate systems, although the normalized element coordinates represent already curvilinear convective coordinates.

An alternative way is to develop the non-linear *geometrically exact* solid-shell elements based on the curvilinear reference surface coordinates that finds its point of departure in papers [12–16]. The term "geometrically exact" reflects the fact that reference surface geometry is described by analytically given functions. Such elements are very promising due to the fact that in the geometric modeling of modern CAD systems the surfaces are usually generated by non-uniform rational B-splines (NURBS) [17,18]. Allowing for that surfaces are conventionally produced by the position vector with representation of two parameters, we can connect the geometric modeling of the shell surface, generated in the CAD system, to the finite

* Corresponding author. Tel.: +7 475 253 2017; fax: +7 475 271 0216.
E-mail addresses: kulikov@apmath.tstu.ru, gmkulikov@mail.ru (G.M. Kulikov).
URL: http://apm.tstu.ru/kulikov.

0168-874X/$ - see front matter © 2007 Elsevier B.V. All rights reserved.
doi:10.1016/j.finel.2006.11.003

element analysis of shell structures. So, it is advantageous to use NURBS shell surface functions directly in the shell calculations and geometrically exact solid-shell elements are best suited for this purpose. They also have the two-parameter representation in surfaces and all geometric computations may be done in the reference surface using NURBS surface representations in the CAD system.

The solid-shell element formulation developed is based on the new non-linear strain–displacement relationships of the first-order six-parameter shell theory. It is remarkable that these strain–displacement relationships precisely represent arbitrarily large rigid-body motions and no assumptions except for standard Timoshenko–Mindlin kinematics are required to derive them. For this purpose displacement vectors of the bottom and top surfaces of the shell are introduced but resolved, in contrast with the isoparametric solid-shell element formulation [1–10], in the reference surface frame. One can compare the proposed non-linear shell formulation with the finite element formulation of Simo et al. [2], where geometrically exact solid-shell elements have been also developed but displacement vectors are resolved in the global Cartesian basis. Therefore, Christoffel symbols and coefficients of the second fundamental form do not explicitly appear in the formulation. This restriction does not give an opportunity to employ the above NURBS surface function technique directly.

The finite element formulation is based on the simple and efficient approximation of shells via four-node curved shell elements. To avoid shear and membrane locking and have no spurious zero energy modes, the assumed strain and stress resultant fields are invoked. This approach was proposed by Wempner et al. [19] for the linear shear deformation shell theory and further was extended by Kulikov and Plotnikova to the geometrically non-linear Timoshenko beam [12], Mindlin plate [13] and Timoshenko–Mindlin shell [14,15] theories allowing for the thickness change. It is known that a six-parameter shell formulation on the basis of the complete 3D constitutive equations is deficient because thickness locking can occur [11]. To prevent thickness locking at the finite element level the enhanced assumed strain method [3,4] can be applied. In order to circumvent a locking phenomenon at both the mechanical and computational levels, the 3D constitutive equations have to be modified. For this purpose the ad hoc modified laminate constitutive stiffness matrix [1,6,20,21], corresponding to the generalized plane stress condition, may be employed. Herein, the second remedy is introduced into the solid-shell formulation.

In the present work compared to earlier authors' shell developments a less number of fundamental unknowns are chosen. This allowed us to elaborate the more robust numerical algorithm. The unknowns consist of six displacements of the bottom and top surfaces of the shell, and nine assumed strains of the face and middle surfaces, and nine conjugate stress resultants instead of 11 assumed strains and 11 stress resultants adopted in [14–16]. Therefore, for deriving element characteristic arrays the Hu–Washizu variational principle has to be applied. The developed formulation is free of assumptions of small displacements, small rotations and small loading steps because it is based on the objective *fully* non-linear strain–displacement equations. There exists only one limitation that a loading step cannot be too large. This restriction arises in the case of using the Newton–Raphson method, since the iteration process can be diverged due to an escape of the initial guess (a result of solving the geometrically linear problem) from Newton's attractive area. Besides, due to the fact that no rotational degrees of freedom (DOF) are introduced, the proposed geometrically exact assumed stress–strain solid-shell element formulation permits, as [6,10,22], to use much larger load increments compared to conventional displacement-based finite element formulations.

The paper focuses on the enhanced non-linear solid-shell formulation through using the ANS method. The main idea of such formulation can be traced back to the ANS method [23,24] developed by many investigators for the linear and non-linear displacement, mixed and hybrid isoparametric finite element formulations [2,5,7,8,10,25,26]. In contrast with above investigations, we treat the term "ANS method" in the broad sense [12,16]. In our formulation all in-plane and transverse components of the natural strain tensor are assumed to vary bilinearly inside the element. Thus, no expected biquadratic interpolation typical for the non-linear four-node solid-shell element is used. The advantages of the proposed non-linear finite element formulation for *coarse meshes* are discussed in all benchmark problems.

2. Geometry and kinematic description of shell

Consider a shell built up in the general case by the arbitrary superposition across the wall thickness of N thin layers of the thickness h_k. The kth layer may be defined as a 3D body of volume V_k bounded by two surfaces S_{k-1} and S_k, located at the distances d_{k-1} and d_k measured with respect to the reference surface S, and the edge boundary surface Ω_k as shown in Figs. 1 and 2. The full edge boundary surface $\Omega=\Omega_1+\Omega_2+\cdots+\Omega_N$ is generated by normals to the reference surface along the bounding curve $\Gamma \subset S$. The reference surface is assumed to be continuous, sufficiently smooth and without any singularities. One can see in Fig. 3 that no serious limitation is introduced invoking this assumption because in the case of the robust choice of the reference surface we are able to model shell intersections and to describe shell edges of the general configuration properly. Let the reference surface S be referred to the orthogonal curvilinear coordinates α_1 and α_2, which are referred to the lines of principal curvatures of its surface. It is also supposed that the α_3-coordinate is oriented along the unit vector $\boldsymbol{a}_3=\mathbf{e}_3$ normal to the reference surface; $\boldsymbol{a}_\alpha=A_\alpha\mathbf{e}_\alpha$ are the basis vectors of the reference surface S; $\mathbf{g}_\alpha^\pm=A_\alpha^\pm\mathbf{e}_\alpha$ are the basis vectors of the bottom surface $S^-=S_0$ and top surface $S^+=S_N$; $\mathbf{g}_\alpha^{\mathrm{M}}=A_\alpha^{\mathrm{M}}\mathbf{e}_\alpha$ are the basis vectors of the midsurface S^{M}; $\mathbf{e}_\alpha$ are the tangent unit vectors to the lines of principal curvatures of the reference surface; A_α, $A_\alpha^\pm$ and A_α^{M} are the Lamé coefficients of corresponding surfaces defined as

$$A_\alpha^\pm=A_\alpha\zeta_\alpha^\pm,\quad A_\alpha^{\mathrm{M}}=A_\alpha\zeta_\alpha^{\mathrm{M}},$$
$$\zeta_\alpha^\pm=1+k_\alpha d^\pm,\quad \zeta_\alpha^{\mathrm{M}}=1+k_\alpha d^{\mathrm{M}},$$
$$d^{\mathrm{M}}=(d^-+d^+)/2,\quad d^-=d_0,\quad d^+=d_N, \tag{1}$$

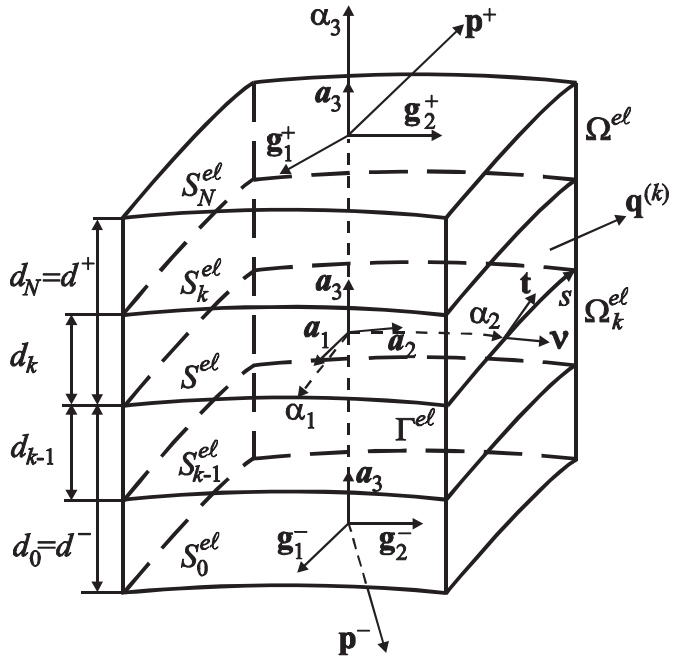

Fig. 1. Multilayered shell element.

where d^{M} is the distance from the reference surface to the midsurface; k_α are the principal curvatures of the reference surface.

The constituent layers of the shell are supposed to be rigidly joined, so that no slip on contact surfaces and no separation of layers can occur. The material of each layer is assumed to be linearly elastic, anisotropic, homogeneous or fiber-reinforced, such that in each point there is a single surface of elastic symmetry parallel to the reference surface. Let p_i^- and p_i^+ be the components of the external loading vectors $\mathbf{p}^-$ and $\mathbf{p}^+$ acting on the bottom and top surfaces in the reference surface frame $\mathbf{e}_i$; $\mathbf{q}^{(k)} = q_\nu^{(k)}\boldsymbol{\nu} + q_t^{(k)}\mathbf{t} + q_3^{(k)}\mathbf{e}_3$ be the external loading vector acting on the edge boundary surface Ω_k, where $q_\nu^{(k)}$, $q_t^{(k)}$ and $q_3^{(k)}$ are the components of its vector in the surface frame $\boldsymbol{\nu}$, $\mathbf{t}$ and $\mathbf{e}_3$; $\boldsymbol{\nu}$ and $\mathbf{t}$ are the normal and tangential unit vectors to the bounding curve Γ. Here and in the following developments the index k identifies the belonging of any quantity to the kth layer and runs from 1 to N; the abbreviation $(\,)_{,\alpha}$ implies the partial derivatives with respect to coordinates α_1 and α_2; indices i, j take the values 1, 2 and 3 while indices α, β, γ take the values 1 and 2.

The position vector $\mathbf{x}$ of the arbitrary point in the shell body can be expressed as

$$\mathbf{x} = N^-\mathbf{x}^- + N^+\mathbf{x}^+, \tag{2a}$$

$$\mathbf{x}^\pm = \mathbf{x}^{\mathrm{R}} + d^\pm\mathbf{e}_3, \tag{2b}$$

$$N^- = \frac{1}{h}(d_N - \alpha_3), \quad N^+ = \frac{1}{h}(\alpha_3 - d_0), \tag{2c}$$

where $\mathbf{x}^{\mathrm{R}}(\alpha_1, \alpha_2)$ is the position vector of the reference surface; $\mathbf{x}^\pm$ are the position vectors of the bottom and top surfaces; $N^\pm(\alpha_3)$ are the linear through-thickness shape functions of the shell; h is the thickness of the shell.

The first-order shell theory is based on the linear approximation of displacements in the thickness direction according to Timoshenko–Mindlin kinematics [27]:

$$\hat{\mathbf{x}} = N^-\hat{\mathbf{x}}^- + N^+\hat{\mathbf{x}}^+, \tag{3a}$$

$$\hat{\mathbf{x}}^\pm = \mathbf{x}^\pm + \mathbf{u}^\pm, \tag{3b}$$

where $\hat{\mathbf{x}}$ and $\hat{\mathbf{x}}^\pm$ are the position vectors of points in the shell body in its current configuration; $\mathbf{u}^\pm(\alpha_1, \alpha_2)$ are the

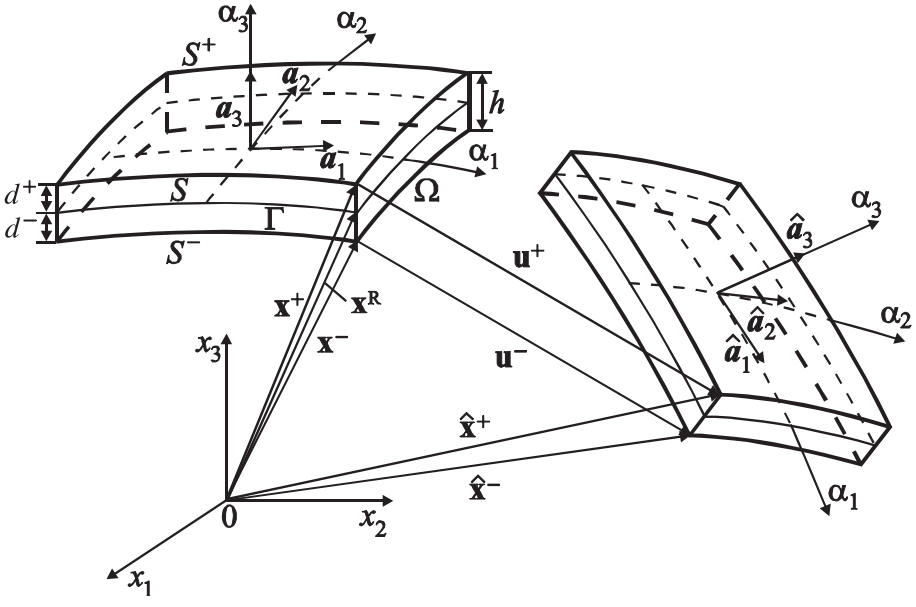

Fig. 2. Geometry and kinematics of shell.

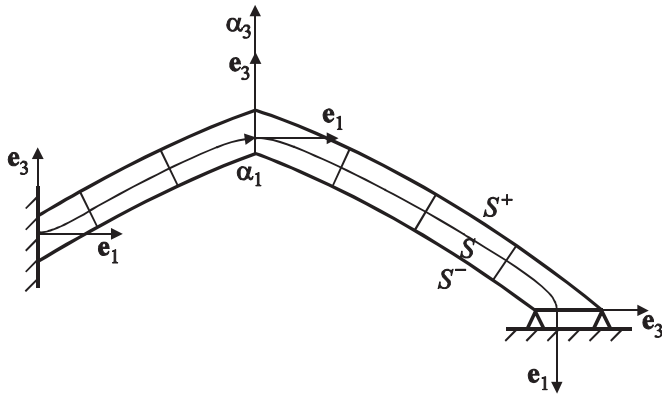

Fig. 3. On the choice of reference surface S.

displacement vectors of the face surfaces defined as

$$\mathbf{u}^{\pm} = \sum_i u_i^{\pm}\mathbf{e}_i. \tag{4}$$

It should be emphasized that displacement vectors are resolved in the reference surface frame $\mathbf{e}_i$. This gives us an opportunity to reduce the costly numerical integration by deriving the stiffness matrix because such a displacement presentation permits to implement the 3D analytical integration [28].

3. Strain–displacement relationships

The components of the Green–Lagrange strain tensor of the finite rotation first-order shell theory can be written as follows [28]:

$$\varepsilon_{\alpha\beta} = L^{-}\varepsilon^{-}_{\alpha\beta} + L^{\mathrm{M}}\varepsilon^{\mathrm{M}}_{\alpha\beta} + L^{+}\varepsilon^{+}_{\alpha\beta}, \tag{5a}$$

$$\varepsilon_{\alpha 3} = N^{-}\varepsilon^{-}_{\alpha 3} + N^{+}\varepsilon^{+}_{\alpha 3}, \tag{5b}$$

$$\varepsilon_{33} = \bar{\varepsilon}_{33}, \tag{5c}$$

$$L^{-} = N^{-}(N^{-} - N^{+}), \quad L^{\mathrm{M}} = 4\,N^{-}N^{+}, \quad L^{+} = N^{+}(N^{+} - N^{-}), \tag{5d}$$

where $L^{\pm}(\alpha_3)$ and $L^{\mathrm{M}}(\alpha_3)$ are the quadratic through-thickness shape functions of the shell; $\varepsilon^{\pm}_{\alpha\beta}$ and $\varepsilon^{\pm}_{\alpha 3}$ are the in-plane and transverse shear strains of the bottom and top surfaces; $\varepsilon^{\mathrm{M}}_{\alpha\beta}$ are the in-plane strains of the midsurface defined as

$$2\varepsilon^{\mathrm{I}}_{\alpha\beta} = \frac{1}{A_\alpha A_\beta}(\hat{\mathbf{g}}^{\mathrm{I}}_\alpha \cdot \hat{\mathbf{g}}^{\mathrm{I}}_\beta - \mathbf{g}^{\mathrm{I}}_\alpha \cdot \mathbf{g}^{\mathrm{I}}_\beta) = \frac{\zeta^{\mathrm{I}}_\beta}{A_\alpha}\mathbf{u}^{\mathrm{I}}_{,\alpha}\cdot\mathbf{e}_\beta + \frac{\zeta^{\mathrm{I}}_\alpha}{A_\beta}\mathbf{u}^{\mathrm{I}}_{,\beta}\cdot\mathbf{e}_\alpha + \frac{1}{A_\alpha A_\beta}\mathbf{u}^{\mathrm{I}}_{,\alpha}\cdot\mathbf{u}^{\mathrm{I}}_{,\beta}, \tag{6a}$$

$$2\varepsilon^{\pm}_{\alpha 3} = \frac{1}{A_\alpha}(\hat{\mathbf{g}}^{\pm}_\alpha \cdot \hat{\boldsymbol{a}}_3 - \mathbf{g}^{\pm}_\alpha \cdot \boldsymbol{a}_3) = \zeta^{\pm}_\alpha \boldsymbol{\beta}\cdot\mathbf{e}_\alpha + \frac{1}{A_\alpha}\mathbf{u}^{\pm}_{,\alpha}\cdot(\mathbf{e}_3 + \boldsymbol{\beta}), \tag{6b}$$

$$2\bar{\varepsilon}_{33} = \hat{\boldsymbol{a}}_3\cdot\hat{\boldsymbol{a}}_3 - \boldsymbol{a}_3\cdot\boldsymbol{a}_3 = 2\boldsymbol{\beta}\cdot(\mathbf{e}_3 + \tfrac{1}{2}\boldsymbol{\beta}), \tag{6c}$$

since the basis vectors in the current shell configuration are

$$\hat{\mathbf{g}}^{\mathrm{I}}_\alpha = \hat{\mathbf{x}}^{\mathrm{I}}_{,\alpha} = \mathbf{g}^{\mathrm{I}}_\alpha + \mathbf{u}^{\mathrm{I}}_{,\alpha}, \quad (\mathrm{I} = -, \mathrm{M}, +), \quad \hat{\boldsymbol{a}}_3 = \boldsymbol{a}_3 + \boldsymbol{\beta}, \tag{7}$$

$$\mathbf{u}^{\mathrm{M}} = \frac{1}{2}(\mathbf{u}^{-} + \mathbf{u}^{+}), \quad \boldsymbol{\beta} = \frac{1}{h}(\mathbf{u}^{+} - \mathbf{u}^{-}), \tag{8}$$

where $\mathbf{u}^{\mathrm{M}}$ is the displacement vector of the midsurface. It is remarkable that strain–displacement relationships (5) and (6) are objective, i.e., invariant under arbitrarily large rigid-body motions. A proof of this statement can be found in [28]. Note also that no assumptions except for Timoshenko–Mindlin kinematics are required to derive them.

The strain terms (5a) quadratic in α_3 can be neglected because of their minor significance in most shell problems. As concerns transverse shear strains (5b), they are considered to be constant in the thickness direction. It is a standard practice in the finite element literature. It should be mentioned that the second assumption is slightly deficient, since some difficulties concerning the implementation of boundary conditions of the hard type may be met. This implies, in particular, that only five of the six strain compatibility equations of the 3D elasticity theory [29] are fulfilled in the case of using a four-node solid-plate element [30]. Nevertheless, we employ these strains in the finite element formulation because of their simplicity

$$\varepsilon_{\alpha\beta} = N^{-}\varepsilon^{-}_{\alpha\beta} + N^{+}\varepsilon^{+}_{\alpha\beta}, \tag{9a}$$

$$\varepsilon_{\alpha 3} = \bar{\varepsilon}_{\alpha 3}, \tag{9b}$$

$$\varepsilon_{33} = \bar{\varepsilon}_{33}, \tag{9c}$$

where $\bar{\varepsilon}_{\alpha 3}$ are the transverse shear strains of the midsurface, which can be expressed according to (1) and (7) in a form

$$2\bar{\varepsilon}_{\alpha 3} = \frac{1}{A_\alpha}(\hat{\mathbf{g}}^{\mathrm{M}}_\alpha \cdot \hat{\boldsymbol{a}}_3 - \mathbf{g}^{\mathrm{M}}_\alpha \cdot \boldsymbol{a}_3) = \zeta^{\mathrm{M}}_\alpha \boldsymbol{\beta}\cdot\mathbf{e}_\alpha + \frac{1}{A_\alpha}\mathbf{u}^{\mathrm{M}}_{,\alpha}\cdot(\mathbf{e}_3 + \boldsymbol{\beta}). \tag{10}$$

Remark 1. In the earlier authors' solid-shell formulation [14–16] instead of (9b) the more general strain distribution (5b) was used. As a result, transverse components of the Green–Lagrange strain tensor (6b) and (6c) satisfy the following coupling conditions:

$$2(\varepsilon^{+}_{\alpha 3} - \varepsilon^{-}_{\alpha 3}) = \frac{1}{A_\alpha} h\bar{\varepsilon}_{33,\alpha}. \tag{11}$$

A proof of this relation is given in [16]. The advantage of strain–displacement relationships (5b), (9a) and (9c) is that all six compatibility equations of the 3D elasticity theory are carried out exactly for all types of solid-plate elements [30]. At the same time the implementation of these relationships for the mixed/hybrid solid-shell elements yields an inclusion additionally of two assumed strains and/or two stress resultants into a set of fundamental unknowns.

Further we represent strain–displacement relations (6) and (10) in a scalar form. Taking into account formulae for the

derivatives of unit vectors $\mathbf{e}_i$ with respect to the orthogonal curvilinear coordinates α_1 and α_2 [31]

$$\frac{1}{A_\alpha}\mathbf{e}_{\alpha,\alpha} = -B_{\alpha\beta}\mathbf{e}_\beta - k_\alpha \mathbf{e}_3, \quad \frac{1}{A_\alpha}\mathbf{e}_{\beta,\alpha} = B_{\alpha\beta}\mathbf{e}_\alpha \quad \text{for } \beta \neq \alpha, \tag{12}$$

$$\frac{1}{A_\alpha}\mathbf{e}_{3,\alpha} = k_\alpha \mathbf{e}_\alpha, \quad B_{\alpha\beta} = \frac{1}{A_\alpha A_\beta}A_{\alpha,\beta},$$

one can write these relations as follows:

$$\varepsilon^{\pm}_{\alpha\beta} = e^{\pm}_{\alpha\beta} + \eta^{\pm}_{\alpha\beta}, \quad \bar{\varepsilon}_{\alpha 3} = \bar{e}_{\alpha 3} + \bar{\eta}_{\alpha 3}, \quad \bar{\varepsilon}_{33} = \bar{e}_{33} + \bar{\eta}_{33}, \tag{13a}$$

$$e^{\pm}_{\alpha\alpha} = \zeta^{\pm}_\alpha \lambda^{\pm}_\alpha, \quad 2e^{\pm}_{12} = \zeta^{\pm}_2 \omega^{\pm}_1 + \zeta^{\pm}_1 \omega^{\pm}_2, \quad 2\bar{e}_{\alpha 3} = \zeta^{\mathrm{M}}_\alpha \beta_\alpha - \theta^{\mathrm{M}}_\alpha,$$
$$\bar{e}_{33} = \beta_3, \tag{13b}$$

$$\eta^{\pm}_{\alpha\alpha} = \tfrac{1}{2}[(\lambda^{\pm}_\alpha)^2 + (\omega^{\pm}_\alpha)^2 + (\theta^{\pm}_\alpha)^2],$$
$$2\eta^{\pm}_{12} = \lambda^{\pm}_1 \omega^{\pm}_2 + \lambda^{\pm}_2 \omega^{\pm}_1 + \theta^{\pm}_1 \theta^{\pm}_2,$$

$$2\bar{\eta}_{\alpha 3} = \beta_\alpha \lambda^{\mathrm{M}}_\alpha + \beta_\gamma \omega^{\mathrm{M}}_\alpha - \beta_3 \theta^{\mathrm{M}}_\alpha \quad \text{for } \gamma \neq \alpha,$$

$$\bar{\eta}_{33} = \tfrac{1}{2}(\beta_1^2 + \beta_2^2 + \beta_3^2), \tag{13c}$$

where

$$\lambda^{\mathrm{I}}_\alpha = \left(\frac{1}{A_\alpha}u^{\mathrm{I}}_\alpha\right)_{,\alpha} + B_{\alpha\alpha}u^{\mathrm{I}}_\alpha + B_{\alpha\beta}u^{\mathrm{I}}_\beta + k_\alpha u^{\mathrm{I}}_3 \quad \text{for } \beta \neq \alpha,$$
$$\omega^{\mathrm{I}}_\alpha = \left(\frac{1}{A_\alpha}u^{\mathrm{I}}_\beta\right)_{,\alpha} + B_{\alpha\alpha}u^{\mathrm{I}}_\beta - B_{\alpha\beta}u^{\mathrm{I}}_\alpha \quad \text{for } \beta \neq \alpha,$$
$$\theta^{\mathrm{I}}_\alpha = -\left(\frac{1}{A_\alpha}u^{\mathrm{I}}_3\right)_{,\alpha} - B_{\alpha\alpha}u^{\mathrm{I}}_3 + k_\alpha u^{\mathrm{I}}_\alpha,$$
$$u^{\mathrm{M}}_i = \frac{1}{2}(u^-_i + u^+_i), \quad \beta_i = \frac{1}{h}(u^+_i - u^-_i), \tag{14}$$

where the superscript $\mathrm{I} = -, \mathrm{M}, +$. It should be mentioned that derivatives in relations (14) have been written in a form that is best suited for applying the analytical integration inside the element.

4. Hu–Washizu variational equation

The finite rotation first-order shell theory developed is based on the assumed approximations of displacements (3) and displacement-dependent strains (9) in the thickness direction. Additionally, for the better computational efficiency we adopt the similar approximation for the displacement-independent strains

$$\varepsilon^{\mathrm{AS}}_{\alpha\beta} = N^- E^-_{\alpha\beta} + N^+ E^+_{\alpha\beta}, \tag{15a}$$

$$\varepsilon^{\mathrm{AS}}_{\alpha 3} = E_{\alpha 3}, \tag{15b}$$

$$\varepsilon^{\mathrm{AS}}_{33} = E_{33}. \tag{15c}$$

Substituting approximations (3), (9) and (15) into the 3D Hu–Washizu variational principle and accounting for that metrics of all surfaces parallel to the reference surface are identical and equal to the metric of the midsurface, one can derive

$$\int\int_S [(\mathbf{H} - \mathbf{D}\mathscr{E})^{\mathrm{T}}\delta\mathbf{E} + (\mathbf{E} - \mathscr{E})^{\mathrm{T}}\delta\mathbf{H} - \mathbf{H}^{\mathrm{T}}\delta\mathscr{E} + \mathbf{P}^{\mathrm{T}}\delta\mathbf{v}]$$
$$\times A^{\mathrm{M}}_1 A^{\mathrm{M}}_2 \,\mathrm{d}\alpha_1\,\mathrm{d}\alpha_2 + \oint_\Gamma \hat{\mathbf{H}}^{\mathrm{T}}_\Gamma \delta\mathbf{v}_\Gamma (1 + k_N d^{\mathrm{M}})\,\mathrm{d}s = 0. \tag{16}$$

Here, matrix notations are introduced

$$\mathbf{v} = [u^-_1 \;\; u^+_1 \;\; u^-_2 \;\; u^+_2 \;\; u^-_3 \;\; u^+_3]^{\mathrm{T}},$$
$$\mathbf{v}_\Gamma = [u^-_\nu \;\; u^+_\nu \;\; u^-_t \;\; u^+_t \;\; u^-_3 \;\; u^+_3]^{\mathrm{T}},$$
$$\mathscr{E} = [\varepsilon^-_{11} \;\; \varepsilon^+_{11} \;\; \varepsilon^-_{22} \;\; \varepsilon^+_{22} \;\; 2\varepsilon^-_{12} \;\; 2\varepsilon^+_{12} \;\; 2\bar{\varepsilon}_{13} \;\; 2\bar{\varepsilon}_{23} \;\; \bar{\varepsilon}_{33}]^{\mathrm{T}},$$
$$\mathbf{E} = [E^-_{11} \;\; E^+_{11} \;\; E^-_{22} \;\; E^+_{22} \;\; 2E^-_{12} \;\; 2E^+_{12} \;\; 2E_{13} \;\; 2E_{23} \;\; E_{33}]^{\mathrm{T}},$$
$$\mathbf{H} = [H^-_{11} \;\; H^+_{11} \;\; H^-_{22} \;\; H^+_{22} \;\; H^-_{12} \;\; H^+_{12} \;\; H_{13} \;\; H_{23} \;\; H_{33}]^{\mathrm{T}},$$
$$\hat{\mathbf{H}}_\Gamma = [\hat{H}^-_{\nu\nu} \;\; \hat{H}^+_{\nu\nu} \;\; \hat{H}^-_{\nu t} \;\; \hat{H}^+_{\nu t} \;\; \hat{H}^-_{\nu 3} \;\; \hat{H}^+_{\nu 3}]^{\mathrm{T}},$$
$$\mathbf{P} = [-p^-_1 \;\; p^+_1 \;\; -p^-_2 \;\; p^+_2 \;\; -p^-_3 \;\; p^+_3]^{\mathrm{T}}, \tag{17}$$

where $\mathbf{D}$ is the ad hoc modified laminate constitutive stiffness matrix corresponding to the generalized plane stress condition [6,20], whose components are defined according to [21], in order to overcome thickness locking; $u^{\pm}_\nu$, $u^{\pm}_t$ and $u^{\pm}_3$ are the components of the displacement vectors of the face surfaces in the coordinate system ν, t and α_3 (Fig. 1); k_N is the normal curvature of the bounding curve Γ; $H^{\pm}_{\alpha\beta}$ and H_{i3} are the stress resultants; $\hat{H}^{\pm}_{\nu\nu}$, $\hat{H}^{\pm}_{\nu t}$ and $\hat{H}^{\pm}_{\nu 3}$ are the external load resultants given by

$$H^{\pm}_{\alpha\beta} = \sum_k \int_{d_{k-1}}^{d_k} S^{(k)}_{\alpha\beta} N^{\pm}\,\mathrm{d}\alpha_3, \quad H_{i3} = \sum_k \int_{d_{k-1}}^{d_k} S^{(k)}_{i3}\,\mathrm{d}\alpha_3,$$

$$\hat{H}^{\pm}_{\nu\text{æ}} = \sum_k \int_{d_{k-1}}^{d_k} q^{(k)}_{\text{æ}} N^{\pm}\,\mathrm{d}\alpha_3 \quad (\text{æ} = \nu, \mathrm{t} \text{ and } 3), \tag{18}$$

where $S^{(k)}_{ij}$ are the components of the second Piola–Kirchhoff stress tensor of the kth layer.

5. Finite element formulation

The mixed variational equation (16) for the shell element, depicted in Fig. 4, can be written as

$$\int_{-1}^{1}\int_{-1}^{1} [\delta\mathbf{E}^{\mathrm{T}}(\mathbf{H} - \mathbf{D}\mathbf{E}) + \delta\mathbf{H}^{\mathrm{T}}(\mathbf{E} - \mathscr{E}) - \delta\mathscr{E}^{\mathrm{T}}\mathbf{H} + \delta\mathbf{v}^{\mathrm{T}}\mathbf{P}]$$
$$\times A^{e\ell}_1 A^{e\ell}_2 \zeta^{\mathrm{M}}_1 \zeta^{\mathrm{M}}_2 \,\mathrm{d}\xi_1\,\mathrm{d}\xi_2$$
$$+ \oint_{\Gamma^{e\ell}} \delta\mathbf{v}^{\mathrm{T}}_\Gamma \hat{\mathbf{H}}_\Gamma (1 + k_N d^{\mathrm{M}})\,\mathrm{d}s = 0, \tag{19}$$

where $A^{e\ell}_\gamma = A_\gamma \ell^{e\ell}_\gamma$ are the Lamé coefficients of the reference surface of the element $S^{e\ell}$; $\xi_\gamma = (\alpha_\gamma - c^{e\ell}_\gamma)/\ell^{e\ell}_\gamma$ are the curvilinear normalized coordinates (natural coordinates in our shell formulation); $c^{e\ell}_\gamma = (\alpha^{-e\ell}_\gamma + \alpha^{+e\ell}_\gamma)/2$ are the coordinates of the

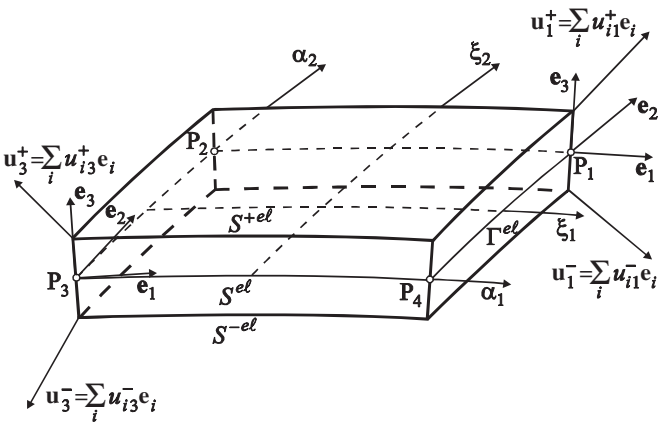

$P_1\left(\alpha_1^{+el},\alpha_2^{+el}\right)$, $P_2\left(\alpha_1^{-el},\alpha_2^{+el}\right)$, $P_3\left(\alpha_1^{-el},\alpha_2^{-el}\right)$, $P_4\left(\alpha_1^{+el},\alpha_2^{-el}\right)$ are the nodal points of the element

Fig. 4. Four-node curved solid-shell element.

center of the element; $2\ell_\gamma^{el}=\alpha_\gamma^{+el}-\alpha_\gamma^{-el}$ are the lengths of the element.

5.1. Assumed stress–strain formulation

For the simplest four-node *curved* solid-shell element the displacement field is approximated according to the standard C^0 interpolation

$$\mathbf{v}=\sum_r N_r\mathbf{v}_r,\quad \mathbf{v}_r=[u_{1r}^-\ u_{1r}^+\ u_{2r}^-\ u_{2r}^+\ u_{3r}^-\ u_{3r}^+]^{\mathrm{T}} \tag{20}$$

or

$$\begin{aligned}
&\mathbf{v}=\sum_{r_1,r_2}\xi_1^{r_1}\xi_2^{r_2}\mathbf{v}^{r_1r_2},\\
&\mathbf{v}^{00}=\tfrac{1}{4}(\mathbf{v}_1+\mathbf{v}_2+\mathbf{v}_3+\mathbf{v}_4),\quad \mathbf{v}^{10}=\tfrac{1}{4}(\mathbf{v}_1-\mathbf{v}_2-\mathbf{v}_3+\mathbf{v}_4),\\
&\mathbf{v}^{01}=\tfrac{1}{4}(\mathbf{v}_1+\mathbf{v}_2-\mathbf{v}_3-\mathbf{v}_4),\\
&\mathbf{v}^{11}=\tfrac{1}{4}(\mathbf{v}_1-\mathbf{v}_2+\mathbf{v}_3-\mathbf{v}_4),
\end{aligned} \tag{21}$$

where $\mathbf{v}_r$ are the displacement vectors of the element nodes; $N_r(\xi_1,\xi_2)$ are the bilinear shape functions of the element; the index r denotes a number of nodes and ranges from 1 to 4 and throughout this section superscripts r_1, r_2, r_3 and r_4 take the values 0 and 1. The surface traction vector is also assumed to vary bilinearly inside the element.

Using (21) in relations (13) and (14) leads to the biquadratic interpolation for displacement-dependent strains

$$\boldsymbol{\mathscr{E}}=\sum_{s_1,s_2}\xi_1^{s_1}\xi_2^{s_2}\boldsymbol{\mathscr{E}}^{s_1s_2}, \tag{22a}$$

$$\begin{aligned}
\boldsymbol{\mathscr{E}}^{s_1s_2}=[&\varepsilon_{11}^{-s_1s_2}\ \varepsilon_{11}^{+s_1s_2}\ \varepsilon_{22}^{-s_1s_2}\ \varepsilon_{22}^{+s_1s_2}\ 2\varepsilon_{12}^{-s_1s_2}\ 2\varepsilon_{12}^{+s_1s_2}\ 2\bar{\varepsilon}_{13}^{s_1s_2}\\
&2\bar{\varepsilon}_{23}^{s_1s_2}\ \bar{\varepsilon}_{33}^{s_1s_2}]^{\mathrm{T}},
\end{aligned} \tag{22b}$$

where

$$\varepsilon_{\alpha\beta}^{\pm s_1s_2}=e_{\alpha\beta}^{\pm s_1s_2}+\eta_{\alpha\beta}^{\pm s_1s_2},\quad \bar{\varepsilon}_{i3}^{s_1s_2}=\bar{e}_{i3}^{s_1s_2}+\bar{\eta}_{i3}^{s_1s_2}, \tag{23a}$$

$$\begin{aligned}
&e_{\alpha\alpha}^{\pm r_1r_2}=\{\zeta_\alpha^{\pm}\}^{00}\lambda_\alpha^{\pm r_1r_2},\\
&2e_{12}^{\pm r_1r_2}=\{\zeta_2^{\pm}\}^{00}\omega_1^{\pm r_1r_2}+\{\zeta_1^{\pm}\}^{00}\omega_2^{\pm r_1r_2},
\end{aligned} \tag{23b}$$

$$2\bar{e}_{\alpha3}^{r_1r_2}=\{\zeta_\alpha^{\mathrm{M}}\}^{00}\beta_\alpha^{r_1r_2}-\theta_\alpha^{\mathrm{M}r_1r_2},\quad \bar{e}_{33}^{r_1r_2}=\beta_3^{r_1r_2},$$

$$e_{\alpha\beta}^{\pm s_1s_2}=0\quad\text{and}\quad \bar{e}_{i3}^{s_1s_2}=0\quad\text{for } s_1=2\ \text{or}\ s_2=2,$$

$$\begin{aligned}
\eta_{\alpha\alpha}^{\pm s_1s_2}=&\frac{1}{2}\sum_{\substack{r_1+r_3=s_1\\ r_2+r_4=s_2}}(\lambda_\alpha^{\pm r_1r_2}\lambda_\alpha^{\pm r_3r_4}+\omega_\alpha^{\pm r_1r_2}\omega_\alpha^{\pm r_3r_4}\\
&+\theta_\alpha^{\pm r_1r_2}\theta_\alpha^{\pm r_3r_4}),\\
2\eta_{12}^{\pm s_1s_2}=&\sum_{\substack{r_1+r_3=s_1\\ r_2+r_4=s_2}}(\lambda_1^{\pm r_1r_2}\omega_2^{\pm r_3r_4}+\lambda_2^{\pm r_1r_2}\omega_1^{\pm r_3r_4}\\
&+\theta_1^{\pm r_1r_2}\theta_2^{\pm r_3r_4}),\\
2\bar{\eta}_{\alpha3}^{s_1s_2}=&\sum_{\substack{r_1+r_3=s_1\\ r_2+r_4=s_2}}(\beta_\alpha^{r_1r_2}\lambda_\alpha^{\mathrm{M}r_3r_4}+\beta_\gamma^{r_1r_2}\omega_\alpha^{\mathrm{M}r_3r_4}-\beta_3^{r_1r_2}\theta_\alpha^{\mathrm{M}r_3r_4})\\
&\text{for } \gamma\neq\alpha,\\
\bar{\eta}_{33}^{s_1s_2}=&\frac{1}{2}\sum_{\substack{r_1+r_3=s_1\\ r_2+r_4=s_2}}(\beta_1^{r_1r_2}\beta_1^{r_3r_4}+\beta_2^{r_1r_2}\beta_2^{r_3r_4}\\
&+\beta_3^{r_1r_2}\beta_3^{r_3r_4}),
\end{aligned} \tag{23c}$$

where

$$\lambda_\alpha^{\mathrm{I}r_1r_2}=\left\{\frac{1}{A_\alpha^{e\ell}}u_\alpha^{\mathrm{I}}\right\}_\alpha^{r_1r_2}+\{B_{\alpha\alpha}^{e\ell}u_\alpha^{\mathrm{I}}+B_{\alpha\beta}^{e\ell}u_\beta^{\mathrm{I}}+k_\alpha u_3^{\mathrm{I}}\}^{r_1r_2}$$
$$\text{for } \beta\neq\alpha,$$

$$\omega_\alpha^{\mathrm{I}r_1r_2}=\left\{\frac{1}{A_\alpha^{e\ell}}u_\beta^{\mathrm{I}}\right\}_\alpha^{r_1r_2}+\{B_{\alpha\alpha}^{e\ell}u_\beta^{\mathrm{I}}-B_{\alpha\beta}^{e\ell}u_\alpha^{\mathrm{I}}\}^{r_1r_2}\quad\text{for } \beta\neq\alpha,$$

$$\theta_\alpha^{\mathrm{I}r_1r_2}=-\left\{\frac{1}{A_\alpha^{e\ell}}u_3^{\mathrm{I}}\right\}_\alpha^{r_1r_2}+\{-B_{\alpha\alpha}^{e\ell}u_3^{\mathrm{I}}+k_\alpha u_\alpha^{\mathrm{I}}\}^{r_1r_2}$$
$$(\mathrm{I}=-,\mathrm{M},+),$$

$$\beta_i^{r_1r_2}=\frac{1}{h}\{u_i^+-u_i^-\}^{r_1r_2}. \tag{24}$$

In Eqs. (22) and (23) the superscripts s_1 and s_2 run from 0 to 2, and in accordance with (21) and Fig. 4 convenient mesh notations [16] are employed

$$\begin{aligned}
&\{f\}^{00}=\tfrac{1}{4}[f(P_1)+f(P_2)+f(P_3)+f(P_4)],\\
&\{f\}^{10}=\tfrac{1}{4}[f(P_1)-f(P_2)-f(P_3)+f(P_4)],\\
&\{f\}^{01}=\tfrac{1}{4}[f(P_1)+f(P_2)-f(P_3)-f(P_4)],\\
&\{f\}^{11}=\tfrac{1}{4}[f(P_1)-f(P_2)+f(P_3)-f(P_4)],
\end{aligned}$$

$$\{f\}_1^{00}=\{f\}^{10},\quad \{f\}_1^{01}=\{f\}^{11},\quad \{f\}_1^{10}=\{f\}_1^{11}=0,$$

$$\{f\}_2^{00}=\{f\}^{01},\quad \{f\}_2^{10}=\{f\}^{11},\quad \{f\}_2^{01}=\{f\}_2^{11}=0, \tag{25}$$

where P_r are the nodal points of the element. Note also that derivatives from (14) are evaluated by means of a simple

scheme as

$$\left(\frac{1}{A_1^{e\ell}}u_i^{\mathrm{I}}\right)_{,1} = \left\{\frac{1}{A_1^{e\ell}}u_i^{\mathrm{I}}\right\}^{10} + \xi_2\left\{\frac{1}{A_1^{e\ell}}u_i^{\mathrm{I}}\right\}^{11},$$
$$\left(\frac{1}{A_2^{e\ell}}u_i^{\mathrm{I}}\right)_{,2} = \left\{\frac{1}{A_2^{e\ell}}u_i^{\mathrm{I}}\right\}^{01} + \xi_1\left\{\frac{1}{A_2^{e\ell}}u_i^{\mathrm{I}}\right\}^{11}. \tag{26}$$

Further we represent strain–displacement relationships (23) in a matrix form:

$$\mathscr{E}^{s_1s_2} = (\mathbf{B}^{s_1s_2} + \mathbf{A}^{s_1s_2}\mathbf{V})\mathbf{V}, \quad \mathbf{V} = [\mathbf{v}_1^{\mathrm{T}}\ \mathbf{v}_2^{\mathrm{T}}\ \mathbf{v}_3^{\mathrm{T}}\ \mathbf{v}_4^{\mathrm{T}}]^{\mathrm{T}}, \tag{27}$$

where $\mathbf{V}$ is the displacement vector at nodal points of the element; $\mathbf{B}^{s_1s_2}$ are the *constant* matrices of order 9×24 corresponding to the linear strain–displacement transformation (23b) such that $\mathbf{B}^{s_1s_2} = \mathbf{0}$ for $s_1 = 2$ or $s_2 = 2$; $\mathbf{A}^{s_1s_2}$ are the *constant* 3D arrays of order $9 \times 24 \times 24$ corresponding to the non-linear strain–displacement transformation (23c); $\mathbf{A}^{s_1s_2}\mathbf{V}$ are the matrices of order 9×24 and $\mathbf{HA}^{s_1s_2}$ are the symmetric matrices of order 24×24 to be introduced later, whose components are defined as

$$(\mathbf{A}^{s_1s_2}\mathbf{V})_{n_1n_2} = \sum_{n_3} A^{s_1s_2}_{n_1n_2n_3}V_{n_3},$$
$$(\mathbf{HA}^{s_1s_2})_{n_2n_3} = \sum_{n_1} H_{n_1}A^{s_1s_2}_{n_1n_2n_3},$$
$$A^{s_1s_2}_{n_1n_2n_3} = A^{s_1s_2}_{n_1n_3n_2} \quad (n_1 = \overline{1,9} \text{ and } n_2, n_3 = \overline{1,24}). \tag{28}$$

From (28) follows the noteworthy transformation

$$(\mathbf{A}^{s_1s_2}\mathbf{V})^{\mathrm{T}}\mathbf{H} = (\mathbf{HA}^{s_1s_2})\mathbf{V} \tag{29}$$

to be used in Section 5.3 for evaluating the elemental stiffness matrix.

To avoid shear and membrane locking and have no spurious zero energy modes, the assumed displacement-independent strain and stress resultant fields inside the element are introduced

$$\mathbf{E} = \sum_{r_1,r_2}\xi_1^{r_1}\xi_2^{r_2}\mathbf{Q}^{r_1r_2}\mathbf{E}^{r_1r_2},$$
$$\mathbf{E}^{00} = [E_{11}^{-00}\ \ E_{11}^{+00}\ \ E_{22}^{-00}\ \ E_{22}^{+00}\ \ 2E_{12}^{-00}\ \ 2E_{12}^{+00}2E_{13}^{00}\ \ 2E_{23}^{00}\ \ E_{33}^{00}]^{\mathrm{T}},$$
$$\mathbf{E}^{01} = [E_{11}^{-01}\ \ E_{11}^{+01}\ \ 2E_{13}^{01}\ \ E_{33}^{01}]^{\mathrm{T}},$$
$$\mathbf{E}^{10} = [E_{22}^{-10}\ \ E_{22}^{+10}\ \ 2E_{23}^{10}\ \ E_{33}^{10}]^{\mathrm{T}}, \quad \mathbf{E}^{11} = [E_{33}^{11}], \tag{30a}$$

$$\mathbf{H} = \sum_{r_1,r_2}\xi_1^{r_1}\xi_2^{r_2}\mathbf{Q}^{r_1r_2}\mathbf{H}^{r_1r_2},$$
$$\mathbf{H}^{00} = [H_{11}^{-00}\ \ H_{11}^{+00}\ \ H_{22}^{-00}\ \ H_{22}^{+00}\ \ H_{12}^{-00}\ \ H_{12}^{+00}\ \ H_{13}^{00}\ \ H_{23}^{00}\ \ H_{33}^{00}]^{\mathrm{T}},$$
$$\mathbf{H}^{01} = [H_{11}^{-01}\ \ H_{11}^{+01}\ \ H_{13}^{01}\ \ H_{33}^{01}]^{\mathrm{T}},$$
$$\mathbf{H}^{10} = [H_{22}^{-10}\ \ H_{22}^{+10}\ \ H_{23}^{10}\ \ H_{33}^{10}]^{\mathrm{T}}, \quad \mathbf{H}^{11} = [H_{33}^{11}], \tag{30b}$$

$$\mathbf{Q}^{01} = \begin{bmatrix} 1&0&0&0\\ 0&1&0&0\\ 0&0&0&0\\ 0&0&0&0\\ 0&0&0&0\\ 0&0&0&0\\ 0&0&1&0\\ 0&0&0&0\\ 0&0&0&1 \end{bmatrix}, \quad \mathbf{Q}^{10} = \begin{bmatrix} 0&0&0&0\\ 0&0&0&0\\ 1&0&0&0\\ 0&1&0&0\\ 0&0&0&0\\ 0&0&0&0\\ 0&0&0&0\\ 0&0&1&0\\ 0&0&0&1 \end{bmatrix},$$
$$\mathbf{Q}^{11} = \begin{bmatrix} 0\\0\\0\\0\\0\\0\\0\\0\\1 \end{bmatrix}, \tag{31}$$

where $\mathbf{Q}^{00}$ is the identity matrix of order 9×9; $\mathbf{E}^{00}$ and $\mathbf{H}^{00}$ are the vectors of homogeneous states of the assumed strains and stress resultants; $\mathbf{E}^{01}$, $\mathbf{E}^{10}$, $\mathbf{E}^{11}$ and $\mathbf{H}^{01}$, $\mathbf{H}^{10}$, $\mathbf{H}^{11}$ are the vectors of higher approximation modes.

Note that this approach may be treated as an assumed stress–strain formulation and was proposed by Wempner et al. [19] for the linear shear deformation shell theory without the thickness change. Further developments for the geometrically non-linear Timoshenko beam, Mindlin plate and Timoshenko–Mindlin shell theories with thickness changes can be found in [12–16], where, as already mentioned, the more expensive finite element formulation has been developed. This is due to the fact that transverse shear displacement-dependent and -independent strains [15,16] are distributed through the thickness, in contrast with the present formulation, according to the linear law (see Remark 1).

Substituting approximations (20), (22), (27) and (30) into the mixed variational equation (19) and integrating analytically inside the element, one obtains governing equations of the developed finite element formulation

$$\mathbf{E}^{r_1r_2} = (\mathbf{Q}^{r_1r_2})^{\mathrm{T}}(\mathbf{B}^{r_1r_2} + \mathbf{R}^{r_1r_2}\mathbf{V})\mathbf{V}, \tag{32a}$$

$$\mathbf{H}^{r_1r_2} = (\mathbf{Q}^{r_1r_2})^{\mathrm{T}}\mathbf{D}\mathbf{Q}^{r_1r_2}\mathbf{E}^{r_1r_2}, \tag{32b}$$

$$\sum_{r_1,r_2}\frac{1}{3^{r_1+r_2}}(\mathbf{B}^{r_1r_2} + 2\mathbf{R}^{r_1r_2}\mathbf{V})^{\mathrm{T}}\mathbf{Q}^{r_1r_2}\mathbf{H}^{r_1r_2} = \mathbf{F}, \tag{32c}$$

where $\mathbf{F}$ is the element-wise surface force vector; $\mathbf{R}^{r_1r_2}$ are the 3D arrays of order $9 \times 24 \times 24$ defined as

$$\mathbf{R}^{00} = \mathbf{A}^{00} + \tfrac{1}{3}\mathbf{A}^{02} + \tfrac{1}{3}\mathbf{A}^{20} + \tfrac{1}{9}\mathbf{A}^{22}, \quad \mathbf{R}^{10} = \mathbf{A}^{10} + \tfrac{1}{3}\mathbf{A}^{12},$$
$$\mathbf{R}^{01} = \mathbf{A}^{01} + \tfrac{1}{3}\mathbf{A}^{21}, \quad \mathbf{R}^{11} = \mathbf{A}^{11}. \tag{33}$$

During the analytical integration we have supposed that a product

$$A_1^{e\ell}A_2^{e\ell}\zeta_1^{\mathrm{M}}\zeta_2^{\mathrm{M}} = \{A_1^{e\ell}\ \ A_2^{e\ell}\ \ \zeta_1^{\mathrm{M}}\ \ \zeta_2^{\mathrm{M}}\}^{00}, \tag{34}$$

that is, it does not vary inside the element.

5.2. Modified ANS formulation

It is important that a described geometrically exact four-node solid-shell element is too stiff in the case of using *coarse meshes* and some additional numerical procedure needs to be applied. The best solution of the problem is to employ the modified ANS method [12]. The main idea of such approach can be traced back to the ANS method [23,24] developed by many scientists for the linear and non-linear displacement, hybrid and mixed isoparametric finite element formulations [2,5,7,8,10,25,26]. In contrast with above formulations, we treat the term "ANS method" in the broad sense. In our formulation all in-plane and transverse components of the natural strain tensor are assumed to vary bilinearly inside the element. This implies that instead of the expected biquadratic interpolation (22) the more suitable ANS interpolation will be used.

So, to improve a geometrically non-linear response of the shell, we interpolate the displacement-dependent strains inside the element as follows:

$$\boldsymbol{\mathscr{E}}^{\mathrm{ANS}} = \sum_r N_r \boldsymbol{\mathscr{E}}_r, \tag{35}$$

where $\boldsymbol{\mathscr{E}}_r$ are the displacement-dependent strain vectors of the element nodes whose components are calculated according to (22)–(24). However, it is more convenient to rewrite the adopted ANS interpolation using a notation (22b) in the following form:

$$\begin{aligned}\boldsymbol{\mathscr{E}}^{\mathrm{ANS}} = {} & \boldsymbol{\mathscr{E}}^{00} + \boldsymbol{\mathscr{E}}^{02} + \boldsymbol{\mathscr{E}}^{20} + \boldsymbol{\mathscr{E}}^{22} + \xi_1(\boldsymbol{\mathscr{E}}^{10} + \boldsymbol{\mathscr{E}}^{12}) \\ & + \xi_2(\boldsymbol{\mathscr{E}}^{01} + \boldsymbol{\mathscr{E}}^{21}) + \xi_1\xi_2\boldsymbol{\mathscr{E}}^{11}.\end{aligned} \tag{36}$$

Substituting approximations (20), (30) and (36) into the variational equation (19) and allowing for (27), one derives finite element equations (32), where instead of 3D arrays (33) the following 3D arrays should be used:

$$\begin{aligned}&\mathbf{R}^{00} = \mathbf{A}^{00} + \mathbf{A}^{02} + \mathbf{A}^{20} + \mathbf{A}^{22}, \quad \mathbf{R}^{10} = \mathbf{A}^{10} + \mathbf{A}^{12}, \\ &\mathbf{R}^{01} = \mathbf{A}^{01} + \mathbf{A}^{21}, \quad \mathbf{R}^{11} = \mathbf{A}^{11}.\end{aligned} \tag{37}$$

Comparing (33) and (37) one can observe that all corresponding arrays differ in multipliers $\frac{1}{3}$ and $\frac{1}{9}$. Therefore, no complication is involved into the finite element formulation employing the modified ANS method.

Remark 2. There is a special case of the modified ANS method, when only three transverse components of the natural strain tensor are interpolated, that is,

$$\begin{aligned}\bar{\varepsilon}_{i3}^{\mathrm{ANS}} = {} & \bar{\varepsilon}_{i3}^{00} + \bar{\varepsilon}_{i3}^{02} + \bar{\varepsilon}_{i3}^{20} + \bar{\varepsilon}_{i3}^{22} + \xi_1(\bar{\varepsilon}_{i3}^{10} + \bar{\varepsilon}_{i3}^{12}) \\ & + \xi_2(\bar{\varepsilon}_{i3}^{01} + \bar{\varepsilon}_{i3}^{21}) + \xi_1\xi_2\bar{\varepsilon}_{i3}^{11}.\end{aligned} \tag{38}$$

Remark 3. In order to circumvent curvature thickness locking for the non-linear isoparametric four-node solid-shell element, Betsch and Stein [7] proposed to apply a bilinear interpolation (35) for the transverse normal strain $\bar{\varepsilon}_{33}$. It is apparent that curvature thickness locking is not related to the geometrically exact four-node solid-shell element because it can handle arbitrary geometry of surfaces properly. We advocate the use of the modified ANS method (35) for all components of the natural strain tensor to improve the non-linear response of the thin shell in the case of coarse meshes.

5.3. Incremental total Lagrangian formulation

Up to this moment, no incremental arguments are needed in the total Lagrangian formulation. The incremental displacements, strains and stress resultants are needed for solving non-linear equations (32) on the basis of the Newton–Raphson method. Further, the left superscripts t and $t+\Delta t$ indicate in which configuration at time t or time $t+\Delta t$ a quantity occurs. Then, in accordance with this agreement we have

$$\begin{aligned}&{}^{t+\Delta t}\mathbf{V} = {}^{t}\mathbf{V} + \Delta\mathbf{V}, \quad {}^{t+\Delta t}\mathbf{F} = {}^{t}\mathbf{F} + \Delta\mathbf{F}, \\ &{}^{t+\Delta t}\mathbf{E}^{r_1r_2} = {}^{t}\mathbf{E}^{r_1r_2} + \Delta\mathbf{E}^{r_1r_2}, \\ &{}^{t+\Delta t}\mathbf{H}^{r_1r_2} = {}^{t}\mathbf{H}^{r_1r_2} + \Delta\mathbf{H}^{r_1r_2},\end{aligned} \tag{39}$$

where $\Delta\mathbf{V}$, $\Delta\mathbf{F}$, $\Delta\mathbf{E}^{r_1r_2}$ and $\Delta\mathbf{H}^{r_1r_2}$ are the incremental variables.

Substituting (39) into the governing equations (31) and taking into account that external loads and second Piola–Kirchhoff stresses constitute the self-equilibrated system in a configuration at time t, one can obtain the incremental equations

$$\Delta\mathbf{E}^{r_1r_2} = (\mathbf{Q}^{r_1r_2})^{\mathrm{T}}({}^{t}\mathbf{M}^{r_1r_2} + \mathbf{R}^{r_1r_2}\Delta\mathbf{V})\Delta\mathbf{V}, \tag{40a}$$

$$\Delta\mathbf{H}^{r_1r_2} = \bar{\mathbf{D}}^{r_1r_2}\Delta\mathbf{E}^{r_1r_2}, \tag{40b}$$

$$\begin{aligned}&\sum_{r_1,r_2}\frac{1}{3^{r_1+r_2}}[2(\mathbf{R}^{r_1r_2}\Delta\mathbf{V})^{\mathrm{T}}\mathbf{Q}^{r_1r_2}{}^{t}\mathbf{H}^{r_1r_2} \\ &\quad + ({}^{t}\mathbf{M}^{r_1r_2} + 2\mathbf{R}^{r_1r_2}\Delta\mathbf{V})^{\mathrm{T}}\mathbf{Q}^{r_1r_2}\Delta\mathbf{H}^{r_1r_2}] = \Delta\mathbf{F}.\end{aligned} \tag{40c}$$

Here and in the following developments matrix notations are used

$$\begin{aligned}&\bar{\mathbf{D}}^{r_1r_2} = (\mathbf{Q}^{r_1r_2})^{\mathrm{T}}\mathbf{D}\mathbf{Q}^{r_1r_2}, \quad \mathbf{D}^{r_1r_2} = \mathbf{Q}^{r_1r_2}\bar{\mathbf{D}}^{r_1r_2}(\mathbf{Q}^{r_1r_2})^{\mathrm{T}}, \\ &{}^{t}\mathbf{M}^{r_1r_2} = \mathbf{B}^{r_1r_2} + 2\mathbf{R}^{r_1r_2}{}^{t}\mathbf{V}.\end{aligned} \tag{41}$$

Due to existence of non-linear terms in incremental equations (40), the Newton–Raphson iteration process should be employed:

$$\begin{aligned}&\Delta\mathbf{V}^{[n+1]} = \Delta\mathbf{V}^{[n]} + \Delta\boldsymbol{\mathscr{V}}^{[n]}, \\ &\Delta\mathbf{E}^{r_1r_2[n+1]} = \Delta\mathbf{E}^{r_1r_2[n]} + \Delta\boldsymbol{\mathscr{I}}^{r_1r_2[n]}, \\ &\Delta\mathbf{H}^{r_1r_2[n+1]} = \Delta\mathbf{H}^{r_1r_2[n]} + \Delta\boldsymbol{\mathscr{H}}^{r_1r_2[n]} \quad (n = 0, 1, \ldots).\end{aligned} \tag{42}$$

As a result, we have

$$\begin{aligned}&\Delta\boldsymbol{\mathscr{I}}^{r_1r_2[n]} - (\mathbf{Q}^{r_1r_2})^{\mathrm{T}}\,{}^{t}\mathbf{L}^{r_1r_2[n]}\Delta\boldsymbol{\mathscr{V}}^{[n]} \\ &\quad = (\mathbf{Q}^{r_1r_2})^{\mathrm{T}}({}^{t}\mathbf{L}^{r_1r_2[n]} - \mathbf{R}^{r_1r_2}\Delta\mathbf{V}^{[n]})\Delta\mathbf{V}^{[n]} - \Delta\mathbf{E}^{r_1r_2[n]},\end{aligned} \tag{43a}$$

$$\Delta\boldsymbol{\mathscr{H}}^{r_1r_2[n]} - \bar{\mathbf{D}}^{r_1r_2}\Delta\boldsymbol{\mathscr{I}}^{r_1r_2[n]} = \bar{\mathbf{D}}^{r_1r_2}\Delta\mathbf{E}^{r_1r_2[n]} - \Delta\mathbf{H}^{r_1r_2[n]}, \tag{43b}$$

$$\sum_{r_1,r_2}\frac{1}{3^{r_1+r_2}}[2(\mathbf{R}^{r_1r_2}\Delta\mathscr{V}^{[n]})^{\mathrm{T}}\mathbf{Q}^{r_1r_2}({}^t\mathbf{H}^{r_1r_2}+\Delta\mathbf{H}^{r_1r_2[n]}) + ({}^t\mathbf{L}^{r_1r_2[n]})^{\mathrm{T}}\mathbf{Q}^{r_1r_2}\Delta\mathscr{H}^{r_1r_2[n]}] = \Delta\mathbf{F}-\sum_{r_1,r_2}\frac{1}{3^{r_1+r_2}}[2(\mathbf{R}^{r_1r_2}\Delta\mathbf{V}^{[n]})^{\mathrm{T}}\mathbf{Q}^{r_1r_2}{}^t\mathbf{H}^{r_1r_2} + ({}^t\mathbf{L}^{r_1r_2[n]})^{\mathrm{T}}\mathbf{Q}^{r_1r_2}\Delta\mathbf{H}^{r_1r_2[n]}], \quad (43c)$$

where

$${}^t\mathbf{L}^{r_1r_2[n]} = \mathbf{B}^{r_1r_2}+2\mathbf{R}^{r_1r_2}({}^t\mathbf{V}+\Delta\mathbf{V}^{[n]}) = {}^t\mathbf{M}^{r_1r_2}+2\mathbf{R}^{r_1r_2}\Delta\mathbf{V}^{[n]}. \quad (44)$$

Eliminating incremental strains $\Delta\mathscr{I}^{r_1r_2[n]}$ and stress resultants $\Delta\mathscr{H}^{r_1r_2[n]}$ from (43) and taking into account the transformation (29), one derives a system of linear equations

$$\mathbf{K}\Delta\mathscr{V}^{[n]} = \Delta\mathscr{F}^{[n]}, \quad (45)$$

where

$$\Delta\mathscr{F}^{[n]} = \Delta\mathbf{F}-\sum_{r_1,r_2}\frac{1}{3^{r_1+r_2}}[({}^t\mathbf{L}^{r_1r_2[n]})^{\mathrm{T}}\mathbf{D}^{r_1r_2} \times({}^t\mathbf{L}^{r_1r_2[n]}-\mathbf{R}^{r_1r_2}\Delta\mathbf{V}^{[n]}) + 2(\mathbf{Q}^{r_1r_2}{}^t\mathbf{H}^{r_1r_2})\mathbf{R}^{r_1r_2}]\Delta\mathbf{V}^{[n]} \quad (46)$$

and $\mathbf{K}=\mathbf{K}_{\mathrm{D}}+\mathbf{K}_{\mathrm{H}}$ denotes the elemental stiffness matrix defined as

$$\mathbf{K}_{\mathrm{D}} = \sum_{r_1,r_2}\frac{1}{3^{r_1+r_2}}({}^t\mathbf{L}^{r_1r_2[n]})^{\mathrm{T}}\mathbf{D}^{r_1r_2}{}^t\mathbf{L}^{r_1r_2[n]}, \quad (47a)$$

$$\mathbf{K}_{\mathrm{H}} = 2\sum_{r_1,r_2}\frac{1}{3^{r_1+r_2}}(\mathbf{Q}^{r_1r_2}{}^t\mathbf{H}^{r_1r_2}+\mathbf{Q}^{r_1r_2}\Delta\mathbf{H}^{r_1r_2[n]})\mathbf{R}^{r_1r_2}. \quad (47b)$$

Finally, we present a formula that is used in (47b) for the computation of incremental stress resultants at the nth iteration step:

$$\mathbf{Q}^{r_1r_2}\Delta\mathbf{H}^{r_1r_2[n]} = \mathbf{D}^{r_1r_2}[({}^t\mathbf{M}^{r_1r_2}+2\mathbf{R}^{r_1r_2}\Delta\mathbf{V}^{[n-1]})\Delta\mathbf{V}^{[n]} - (\mathbf{R}^{r_1r_2}\Delta\mathbf{V}^{[n-1]})\Delta\mathbf{V}^{[n-1]}]. \quad (48)$$

This formula holds for $n\geqslant 1$ while at the beginning of the first iteration one should set

$$\Delta\mathbf{V}^{[0]}=\mathbf{0} \quad \text{and} \quad \Delta\mathbf{H}^{r_1r_2[0]}=\mathbf{0}. \quad (49)$$

Remark 4. The element stiffness matrix possesses a correct rank because 18 assumed strain parameters are adopted according to (30a). It is worth noting that elemental matrices (47) require only direct substitutions, i.e., no inversion is needed to derive them. Furthermore, they are evaluated by using the analytical integration.

The equilibrium equations (45)–(47) for each element are assembled by the usual technique to form the global incremental equilibrium equations. These incremental equations should be performed until the required accuracy of the solution can be obtained. Herein, two convergence criteria are employed to describe more carefully high potential of the proposed finite element formulation, namely,

$$\|\Delta\mathbf{U}^{[n+1]}-\Delta\mathbf{U}^{[n]}\|<\varepsilon\|\Delta\mathbf{U}^{[n]}\| \quad (50)$$

and

$$\|\mathbf{r}^{[n]}\|<\varepsilon\|\mathbf{r}^{[0]}\|, \quad (51)$$

where $\|\bullet\|$ stands for the Euclidean norm; $\Delta\mathbf{U}$ is the global vector of displacement increments; $\mathbf{r}$ is the residual vector; ε is the prescribed tolerance.

Table 1
Listing of non-linear solid-shell elements

Name	Description
GEX4	Geometrically exact assumed stress–strain four-node solid-shell element developed
GEX4A3	GEX4 element on the basis of the incomplete ANS method according to Eq. (38)
GEX4A6	GEX4 element on the basis of the complete ANS method according to Eq. (36)
ISO4	Isoparametric assumed stress four-node solid-shell element with seven displacement degrees of freedom [9]
ISO4AT	Isoparametric assumed stress four-node solid-shell element on the basis of the conventional ANS method using the total Lagrangian framework [10]
ISO4AU	Isoparametric assumed stress four-node solid-shell element on the basis of the conventional ANS method using the updated Lagrangian framework [10]
ISO8	Isoparametric displacement-based eight-node solid-shell element with a reduced integration [4]
ISO9	Isoparametric assumed strain nine-node solid-shell element [6]

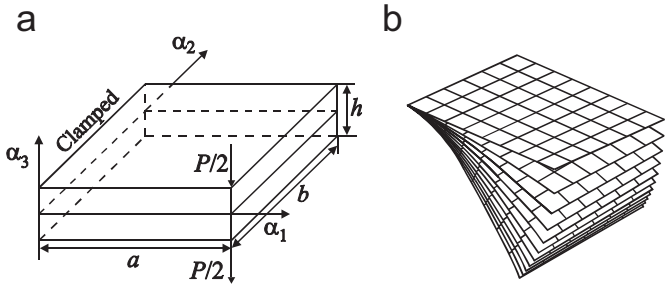

$a=40,\ b=30,\ h=0.4,\ E=1.2\times10^8,\ \nu=0.3,\ P=10^4 f,\ f=4$

Fig. 5. Cantilever plate under concentrated loads at one corner: (a) geometry and (b) deformed configurations (modeled by 8×6 mesh).

6. Benchmark problems

The performance of the proposed geometrically exact solid-shell elements is evaluated with several discriminating problems extracted from the literature. A listing of these elements and the abbreviations used to identify them are contained in Table 1. All our results are compared with those based, as a rule, on using identical node spacing and the same convergence criterion and tolerance. Besides, NStep denotes a number of load

Table 2
Midplane displacements at loaded corner of cantilever plate using 32×24 mesh and residual criterion (51) with tolerance of 10^{-9}

Element	NStep = 1			NStep = 5			NStep = 10		
	u_1^M	u_3^M	NIter	u_1^M	u_3^M	NIter	u_1^M	u_3^M	NIter
GEX4	12.111	26.362	7	12.111	26.362	23	12.111	26.362	41
GEX4A3	12.122	26.375	7	12.122	26.375	23	12.122	26.375	41
GEX4A6	12.121	26.374	7	12.121	26.374	23	12.121	26.374	41

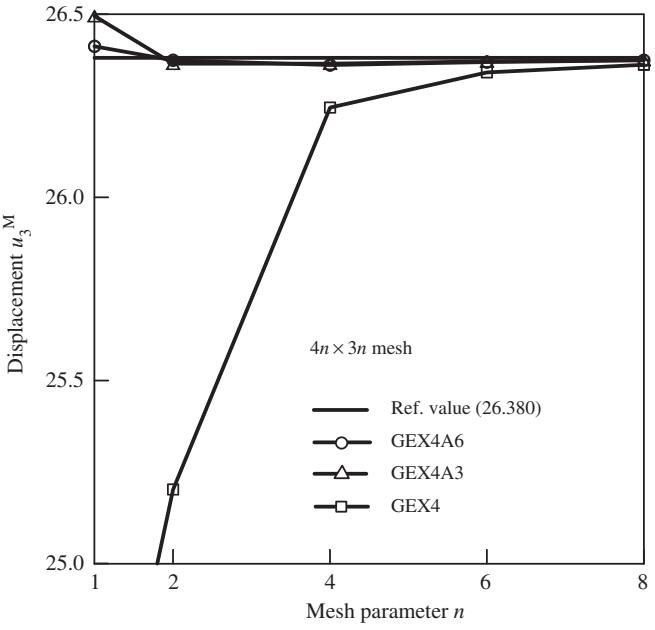

Fig. 6. Convergence study due to mesh refinement for cantilever plate, where reference solution is provided by 64×48 mesh of GEX4A6 elements.

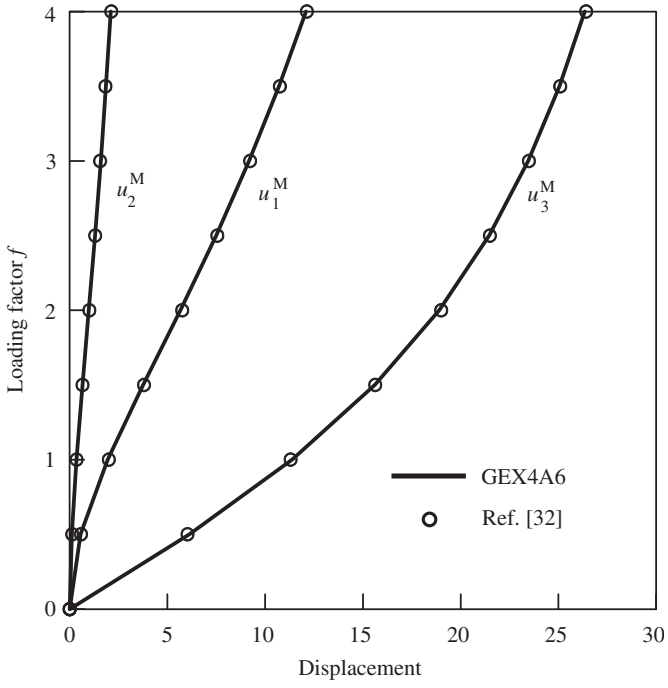

Fig. 7. Midplane displacements under applied loads of cantilever plate (modeled by 8×6 mesh).

steps employed to equally divide the maximum load, whereas NIter stands for a total number of iterations.

The computations were performed on a standard PC Pentium IV using Delphi environment. Note also that all three geometrically exact elements developed are *insensitive* to a number of loading steps.

6.1. Cantilever plate under concentrated loads at one corner

Consider a cantilever isotropic plate subjected at one corner to two conservative transverse forces, acting on the outer planes, as shown in Fig. 5. Such an example has been chosen in order to give one an opportunity to compare geometrically exact solid-shell elements developed with existing isoparametric solid-shell elements. This is due to the simple fact that for the flat plate the proposed analytical integration schemes (23), (24) and (34) yield the *exact integration* because geometrical parameters $A_1 = A_2 = 1$ and $k_1 = k_2 = 0$. As a result only polynomials of the natural coordinates are integrated.

Table 2 lists midplane displacements at the loaded corner. It is seen that predictions of all geometrically exact elements for a fine mesh are very close and insensitive to a number of loading steps but ANS elements are slightly less stiff than the GEX4 element. At the same time, as can be observed in Fig. 6, using coarse meshes leads to a poor performance of the GEX4 element. Additionally, Fig. 7 presents load–displacement curves and a comparison with results reported in [32] employing a finite element formulation with five DOFs per node and five equal load increments. It should be mentioned that converged solutions for our elements can be easily achieved by using only one load step and further loading is possible for all reasonable levels of loading including $P = 4 \times 10^5$ and more.

6.2. Pinched hemispherical shell

To investigate the capability of the proposed geometrically exact elements to model the inextensional bending and rigid-body motions in the case of the exact surface description and spline surface representation as well, we consider one of the most demanding non-linear tests. A hemispherical shell with 18° hole at the top is loaded by two pairs of opposite forces on

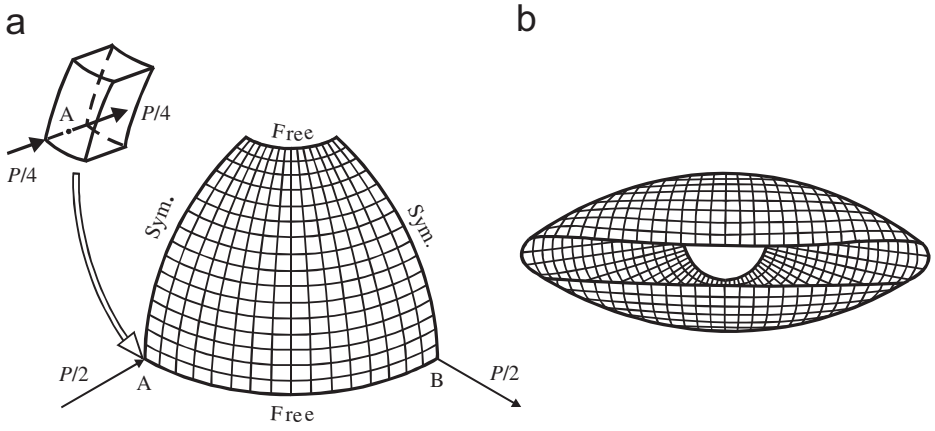

$R=10,\ h=0.04,\ \text{Hole}=18^{\circ},\ E=6.825\times10^{7},\ \nu=0.3,\ P=100\,f,\ f=4$

Shell of revolution with geometrical parameters:
$A_1=R,\ \ A_2=R\cos\alpha_1,\ k_1=k_2=1/R,\ \ \alpha_1\in[0,\ 2\pi/5],\ \alpha_2\in[0,\ \pi/2]$

Fig. 8. Pinched hemispherical shell: (a) geometry and (b) deformed configuration (modeled by 16 × 16 mesh).

Table 3
Midsurface displacements at points A and B of pinched hemispherical shell using 16 × 16 mesh and displacement-based criterion (50) with tolerance of 10^{-4}

Element	NStep = 1			NStep = 5			NStep = 10		
	$-u_3^{\mathrm{M}}$ (A)	u_3^{M} (B)	NIter	$-u_3^{\mathrm{M}}$ (A)	u_3^{M} (B)	NIter	$-u_3^{\mathrm{M}}$ (A)	u_3^{M} (B)	NIter
GEX4	3.8634	7.6079	6	3.8634	7.6079	17	3.8634	7.6079	30
GEX4A3	4.0184	7.9758	7	4.0184	7.9758	17	4.0184	7.9758	29
GEX4A6	4.0557	8.1451	7	4.0557	8.1451	17	4.0557	8.1451	29
ISO4AT	4.0488	8.1173	8	4.0488	8.1173	21	4.0488	8.1173	36
ISO9	4.0205	8.0160	8	4.0209	8.0169	23	4.0209	8.0169	35

the equator. The geometrical and material data of the problem are shown in Fig. 8.

6.2.1. Exact surface representation

The analytical description of the spherical surface is given in Fig. 8. Due to symmetry of the problem, only one quarter of the shell is modeled with regular meshes of developed elements. Table 3 and Fig. 9 display midsurface displacements under applied loads employing geometrically exact and isoparametric solid-shell elements. One can observe that GEX4 and GEX4A3 elements are too stiff in a case of coarse mesh configurations, whereas the GEX4A6 element performs excellently for all meshes because only seven iterations are needed to obtain a solution of this discriminating problem with a prescribed tolerance. Besides, a very coarse mesh 4 × 4 yields 87% of the reference displacement value.

The data in Table 4 exhibit the monotonic convergence of the Newton–Raphson iteration scheme through Euclidean norms of the displacement and residual vectors and an energy variation as well. For the complete picture Fig. 10 presents load–displacement curves compared with those derived by 16 × 16 and 8 × 8 meshes of ISO4AT and ISO9 elements, respectively. As can be seen, all results agree closely but the GEX4A6 element is less expensive owing to the economical derivation of its stiffness matrix.

6.2.2. Spline surface representation

It is apparent that geometrically exact shell elements cannot be readily applied for modeling the shells of free-form surfaces. This is due to the fact that geometric objects such as coefficients of the second fundamental form or curvatures of the reference surface are not easily accessible in a computational context. A methodology of using CAD systems, in particular bicubic B-spline functions, for the modeling of general surface geometry has been recently presented by Roh and Cho [17]. However, for describing the surface of revolution there is no sense to invoke the CAD system technology because in the literature there is a very simple approach based on the cubic spline functions. This approach has been proposed by Grigolyuk and Kulikov as early as 1981 [33] and published later in book [34].

Consider a shell of revolution whose reference surface is generated by rotation of the arbitrary curve C (Fig. 11), given on

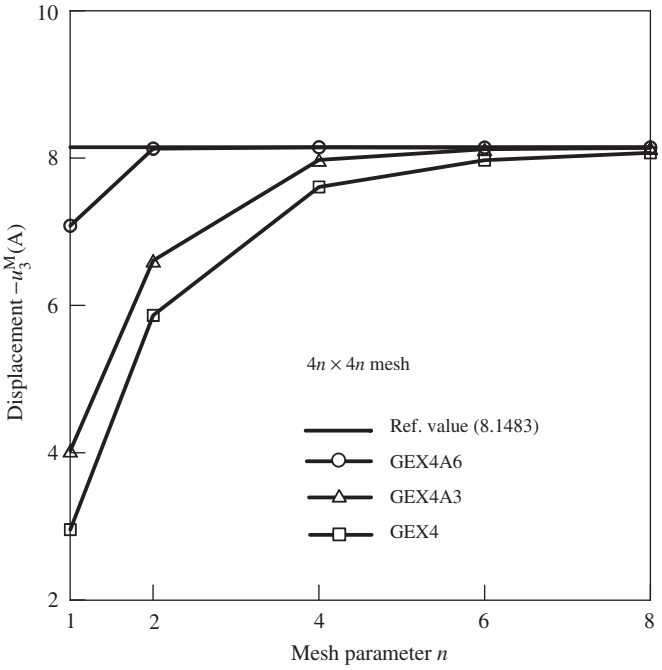

Fig. 9. Convergence study due to mesh refinement for pinched hemispherical shell, where reference solution is provided by 64×64 mesh of GEX4A6 elements.

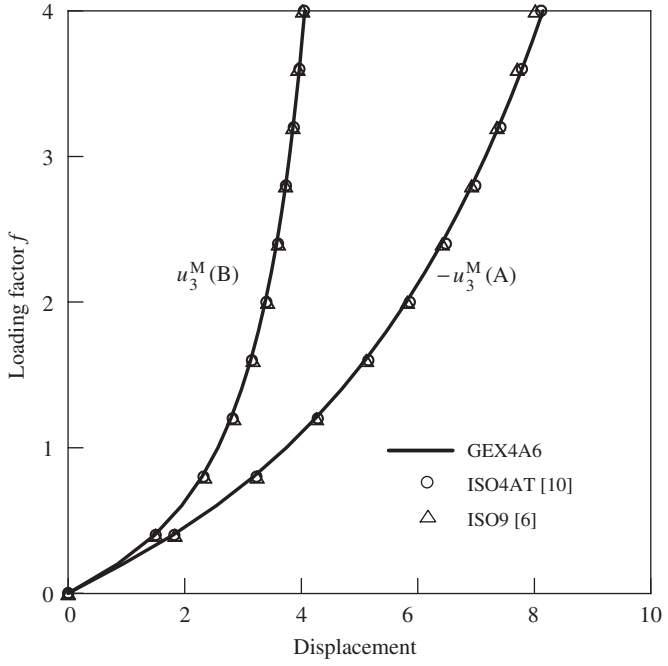

Fig. 10. Midsurface displacements of pinched hemispherical shell (modeled by 16×16 mesh).

Table 4
Convergence results for pinched hemispherical shell employing 16×16 mesh of GEX4A6 elements when total load $P = 400$ is applied in one load step

Iteration	$\|\mathbf{U}^{[n+1]} - \mathbf{U}^{[n]}\|$	$\|\mathbf{r}^{[n]}\|$	$\|W^{[n+1]} - W^{[n]}\|$[a]
0	1.8215E + 2	2.0000E + 2	3.6855E + 3
1	8.5023E + 1	6.4103E + 9	1.5359E + 8
2	3.3183E + 1	8.9031E + 8	1.4530E + 8
3	9.0212E + 0	1.8890E + 8	7.6252E + 6
4	2.2229E + 0	5.3314E + 7	6.6611E + 5
5	6.3550E − 1	3.5903E + 6	4.9016E + 3
6	1.3206E − 2	5.3211E + 4	1.4181E + 0
7	3.1786E − 6	1.5773E + 1	1.7617E − 5
8	4.7285E − 8	5.1482E − 6	2.7882E − 7

[a] W stands for the strain energy.

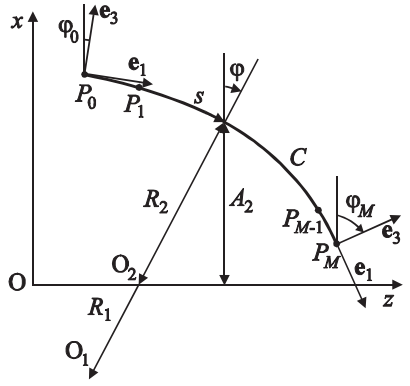

Fig. 11. On the generation of reference surface of revolution.

a plane by a discrete number of prescribed points $P_m(x_m, z_m)$, round the z-axis, where the index m runs from 0 to M. The geometrical parameters of the reference surface can be defined according to [33] as

$$A_1 = 1, \quad A_2 = S_x,$$

$$k_1 = \frac{1}{R_1} = \frac{\mathrm{d}S_x}{\mathrm{d}s}\frac{\mathrm{d}^2S_z}{\mathrm{d}s^2} - \frac{\mathrm{d}S_z}{\mathrm{d}s}\frac{\mathrm{d}^2S_x}{\mathrm{d}s^2}, \quad k_2 = \frac{1}{R_2} = \frac{1}{A_2}\frac{\mathrm{d}S_z}{\mathrm{d}s}, \tag{52}$$

where s is the meridional coordinate; R_1 and R_2 are the principal radii of curvature in the meridional and circumferential directions; $S_x(s)$ and $S_z(s)$ are the cubic spline functions introduced for smoothing the input data (s_m, x_m) and (s_m, z_m), respectively. It is well known that a derivation of the curvature k_1 cannot be carried out simply, since even small errors brought in the values of coordinates x_m and z_m can lead to unacceptable results for the second-order derivatives from (52). To assess the accuracy of this methodology, we introduce the curvature error index as follows:

$$\delta = \left[\sum_{\ell=0}^{\mathscr{L}} (k_{1\ell}^{\text{exact}} - k_{1\ell}^{\text{spline}})^2\right]^{1/2}. \tag{53}$$

As a numerical example we study a sphere whose meridian C is described by a set of equally spaced points given by

$$s_m = 10\varphi_m, \quad x_m = 10\cos\varphi_m, \quad z_m = 10\sin\varphi_m,$$
$$\varphi_m = \pi\left(\frac{m}{M} - \frac{1}{2}\right),$$

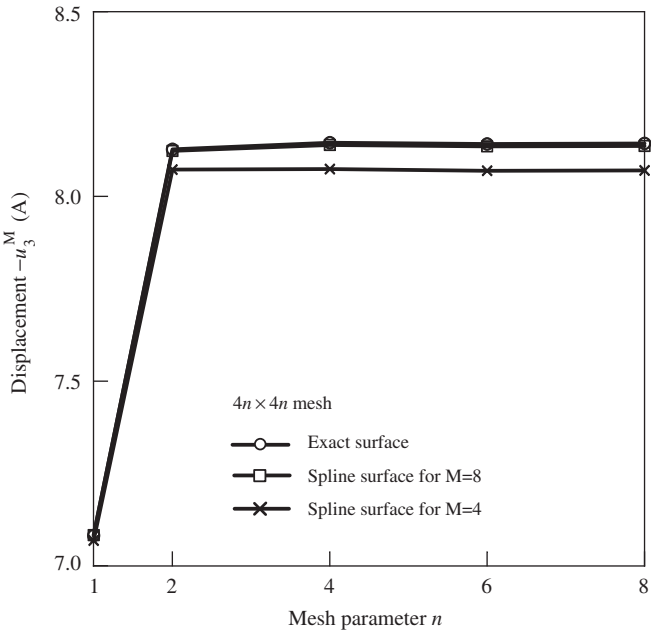

Fig. 12. Convergence study due to mesh refinement for pinched hemispherical shell with GEX4A6 element.

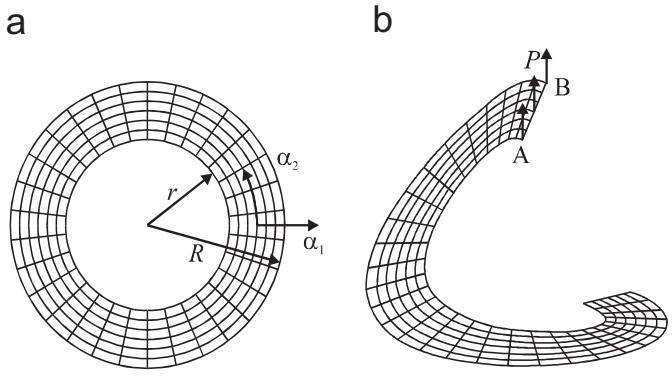

Fig. 13. Slit ring plate under line load: (a) geometry and (b) deformed configuration (modeled by 6 × 30 mesh).

where M=4, 8 and 16, i.e., three different spline representations of the spherical surface are considered and compared with each other. Note that all values of coordinates are rounded off to the second figure after a decimal point. Therefore, the mean deviation of the derived values from their exact ones should be chosen as 0.0029. Let $\mathscr{L}$ from (53) equal 64. In such case the use of the numerical algorithm [33] with boundary tangent angles of ±90° yields the following curvature errors: $\delta = 0.0195$, 0.00639 and 0.00580 for $M = 4$, 8 and 16, respectively. It is seen that results based on spline surface geometry are quite correct even for the small number of prescribed points.

Fig. 12 shows results of the convergence study for the above hemispherical shell with 18° hole based on the GEX4A6 element through spline surfaces with various data points and a comparison with exact geometry as well. One can observe that spline surface computations for $M = 8$ are in a good agreement with exact ones.

6.3. Slit ring plate under line load

This example was presented by Basar and Ding [35] to test non-linear formulations for shell structures and further has been used by many investigators. The ring plate is subjected to a line load P applied at its free edge of the slit while the other edge is fully clamped. The plate is modeled by a shell of revolution with geometrical parameters shown in Fig. 13.

The displacements at points A and B of the plate, presented in Table 5 and Figs. 14 and 15, have been found using uniform meshes of geometrically exact elements. A comparison with results of Sansour et al. [9] and Sze et al. [10] obtained by employing the 6 × 30 mesh of assumed stress four-node solid-shell elements is also given. As can be seen from Fig. 14, we can use extremely coarse meshes with the GEX4A6 element, since a 2 × 4 mesh already yields 92% of the reference solution. At the same time the GEX4 element ignoring the ANS interpolation is too stiff for such coarse mesh configurations.

6.4. Pulled cylindrical shell

A cylindrical shell pulled by a pair of opposite concentrated loads is a very popular non-linear benchmark problem [4,6,9,10]. The geometrical and material data of the shell are given in Fig. 16.

Owing to symmetry of the problem, only one octant of the cylinder is discretized by regular meshes. Table 6 and Figs. 17 and 18 display our results and a comparison with

Table 5
Midplane displacements at points A and B of slit ring plate using 6 × 30 mesh and displacement-based criterion (50) with tolerance of 10^{-4}

Element	NStep = 1			NStep = 5			NStep = 10		
	u_3^M (A)	u_3^M (B)	NIter	u_3^M (A)	u_3^M (B)	NIter	u_3^M (A)	u_3^M (B)	NIter
GEX4	13.407	16.959	13	13.405	16.955	20	13.407	16.959	32
GEX4A3	13.583	17.207	14	13.581	17.202	19	13.583	17.207	31
GEX4A6	13.531	17.164	10	13.527	17.157	19	13.531	17.164	32
ISO4AT	13.618	17.257	11	13.618	17.257	25	13.618	17.257	42
ISO4AU	No convergence			13.623	17.261	28	13.623	17.261	47

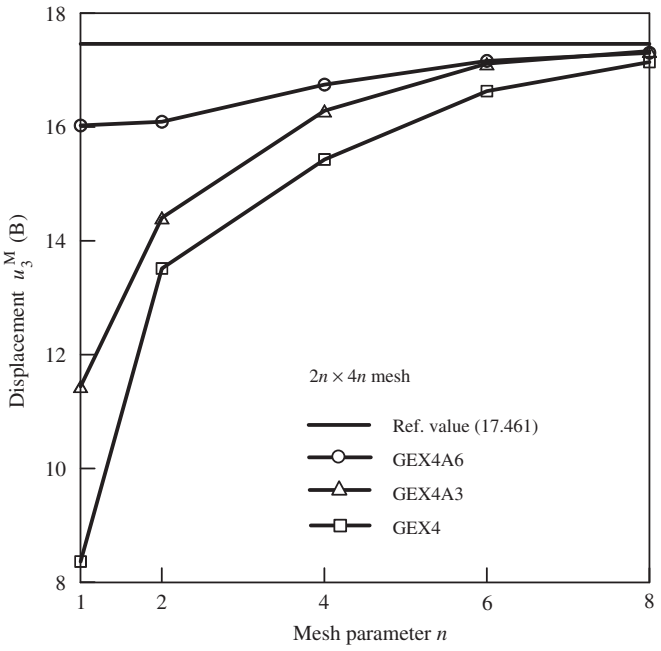

Fig. 14. Convergence study due to mesh refinement for slit ring plate, where reference solution is provided by 32×64 mesh of GEX4A6 elements.

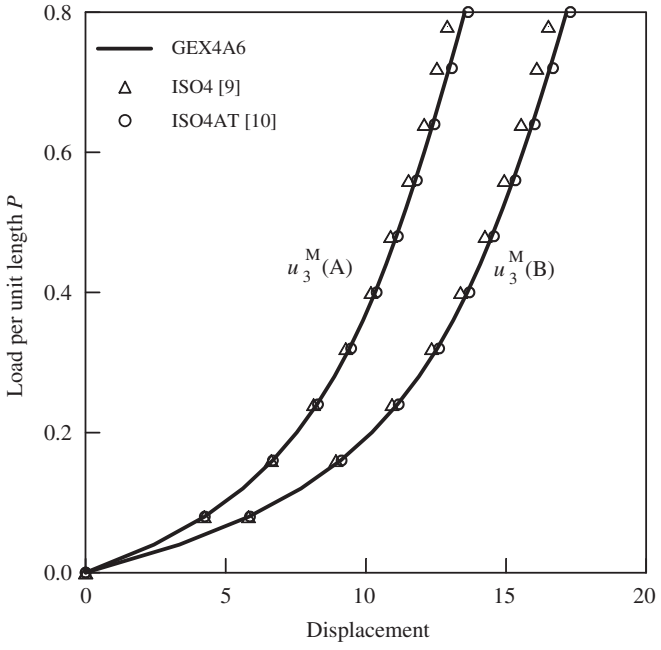

Fig. 15. Midplane displacements of slit ring plate (modeled by 6×30 mesh).

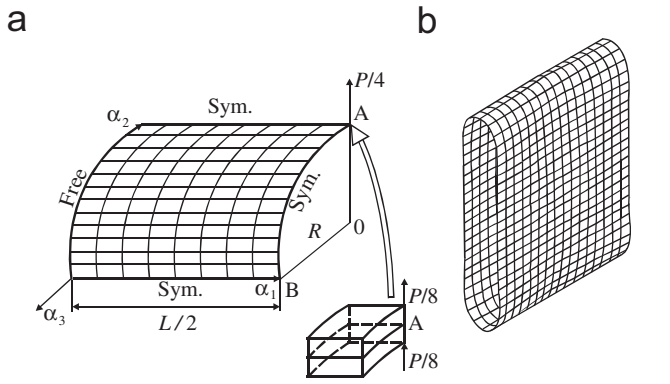

$R = 4.953,\ L = 10.35,\ h = 0.094,\ E = 1.05 \times 10^7,\ \nu = 0.3125,\ P = 10^4 f, f = 1.8$

Shell of revolution with geometrical parameters:
$A_1 = 1,\ A_2 = R,\ k_1 = 0,\ k_2 = 1/R,\ \alpha_1 \in [0, L/2],\ \alpha_2 \in [0, \pi/2]$

Fig. 16. Pulled cylindrical shell: (a) geometry and (b) deformed configuration for $f = 1.95$ (modeled by 8×12 mesh).

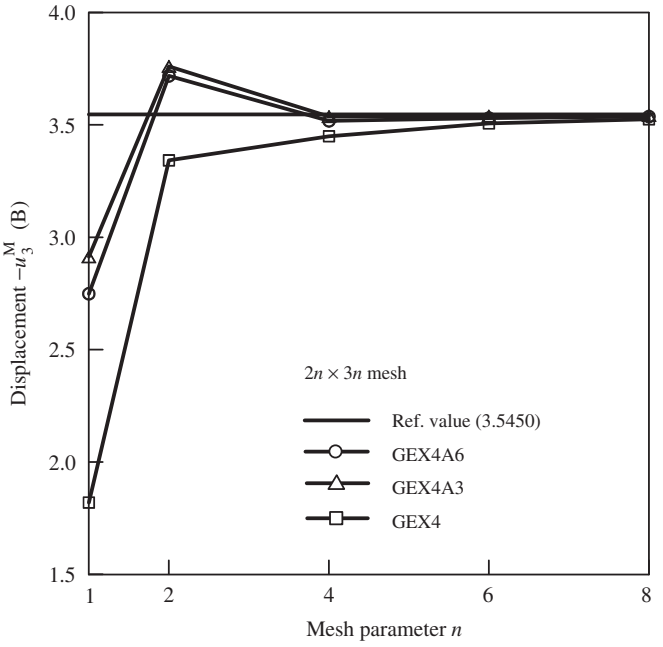

Fig. 17. Convergence study due to mesh refinement for pulled cylindrical shell, where reference solution is provided by 32×48 mesh of GEX4A6 elements.

Table 6
Midsurface displacements at points A and B of pulled cylindrical shell using 32×48 mesh and residual criterion (51) with tolerance of 10^{-10}

Element	NStep = 1			NStep = 5			NStep = 10		
	u_3^M (A)	$-u_3^M$ (B)	NIter	u_3^M (A)	$-u_3^M$ (B)	NIter	u_3^M (A)	$-u_3^M$ (B)	NIter
GEX4	2.4143	3.5423	8	2.4143	3.5423	22	2.4143	3.5423	36
GEX4A3	2.4200	3.5464	8	2.4200	3.5464	22	2.4200	3.5464	36
GEX4A6	2.4173	3.5450	8	2.4173	3.5450	22	2.4173	3.5450	36

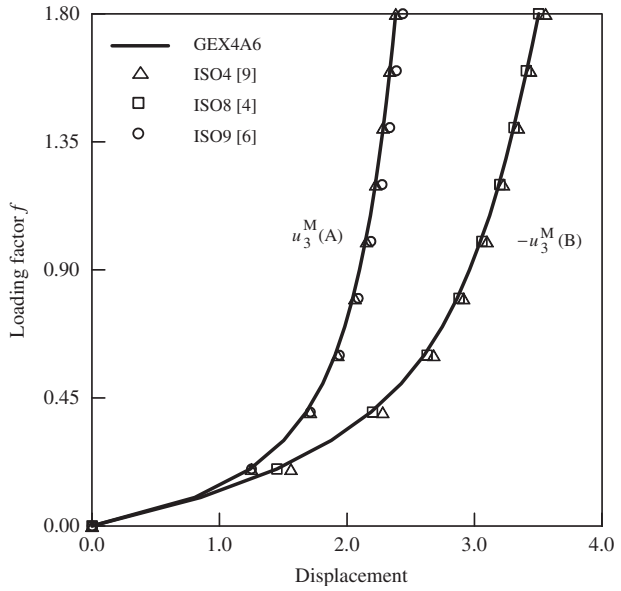

Fig. 18. Midsurface displacements of pulled cylindrical shell (modeled by 8×16 mesh).

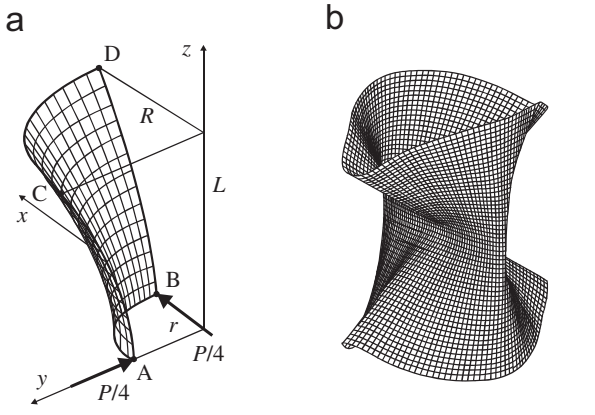

$r=7.5, R=15, L=20, h=0.04, h_0=h/3$

$E_L=4\times10^7$, $E_T=10^6$, $G_{LT}=G_{TT}=6\times10^5$, $\nu_{LT}=\nu_{TT}=0.25$, $P=80f$, $f=5$

Ply thickness = $[h_0/h_0/h_0]$, Ply orientation = [0/90/0] and [90/0/90]

Shell of revolution with geometrical parameters ($\alpha_1=z\in[0, L]$, $\alpha_2\in[0,\pi/2]$):

$$A_1=\sqrt{1+\frac{\mu^2z^2}{A_2^2}},\ A_2=r\sqrt{1+\frac{\mu z^2}{r^2}},\ k_1=-\frac{\mu r^2}{A_1^3A_2},\ k_2=\frac{1}{A_1A_2},\ \mu=\frac{R^2-r^2}{L^2}$$

Fig. 19. Pinched cross-ply hyperbolic shell: (a) geometry and (b) deformed configuration for ply orientation [90/0/90] (modeled by 28×28 mesh).

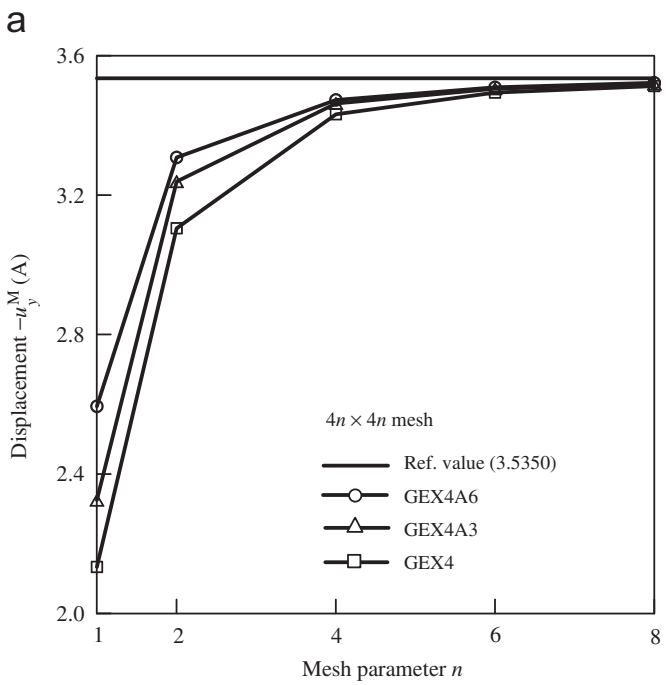

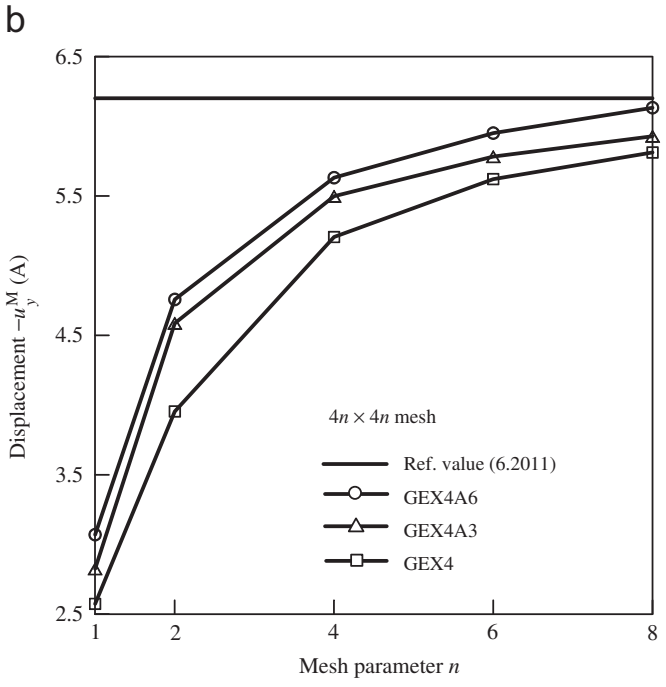

Fig. 20. Convergence study due to mesh refinement for pinched cross-ply hyperbolic shell for ply orientations: (a) [0/90/0] and (b) [90/0/90], where reference solutions are provided by 64×64 mesh of GEX4A6 elements.

Table 7
Midsurface displacements at points A and C of pinched cross-ply hyperbolic shell using 32×32 mesh and residual criterion (51) with tolerance of 10^{-8}

Ply sequence	Element	NStep = 1			NStep = 5			NStep = 10		
		$-u_y^M$(A)	u_y^M(C)	NIter	$-u_y^M$(A)	u_y^M(C)	NIter	$-u_y^M$(A)	u_y^M(C)	NIter
[0/90/0]	GEX4	3.5129	2.5130	8	3.5129	2.5130	18	3.5129	2.5130	32
	GEX4A3	3.5194	2.5161	8	3.5194	2.5161	18	3.5194	2.5161	32
	GEX4A6	3.5215	2.5179	8	3.5215	2.5179	18	3.5215	2.5179	32
[90/0/90]	GEX4	No convergence			5.8121	2.7898	26	5.8121	2.7898	38
	GEX4A3	No convergence			5.9282	2.7874	26	5.9282	2.7874	38
	GEX4A6	No convergence			6.1330	2.6914	31	6.1330	2.6914	40

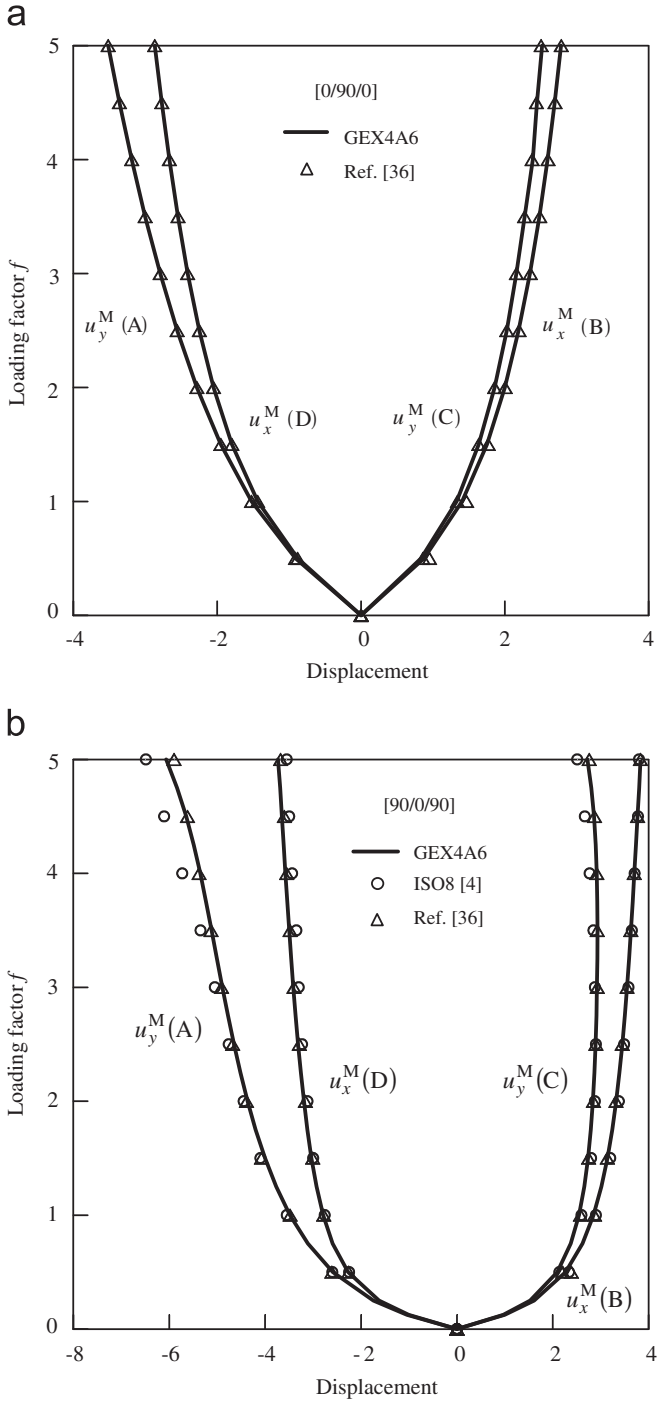

Fig. 21. Midsurface displacements of pinched cross-ply hyperbolic shell for ply orientations: (a) [0/90/0] and (b) [90/0/90] (modeled by 28 × 28 mesh).

those derived by using 8 × 16 and 4 × 8 meshes of bilinear [9] and quadratic [4,6] solid-shell elements. It is interesting that many researchers detected a slight snap-through behavior of the shell. So, Sze et al. [10] found that snap-through occurs when a loading factor f is between 1.9 and 2.0. Since we had no interest to investigate a post-buckling behavior of the shell and taking into consideration the aforementioned result, we stopped our calculations at $f = 1.95$ during a derivation of the

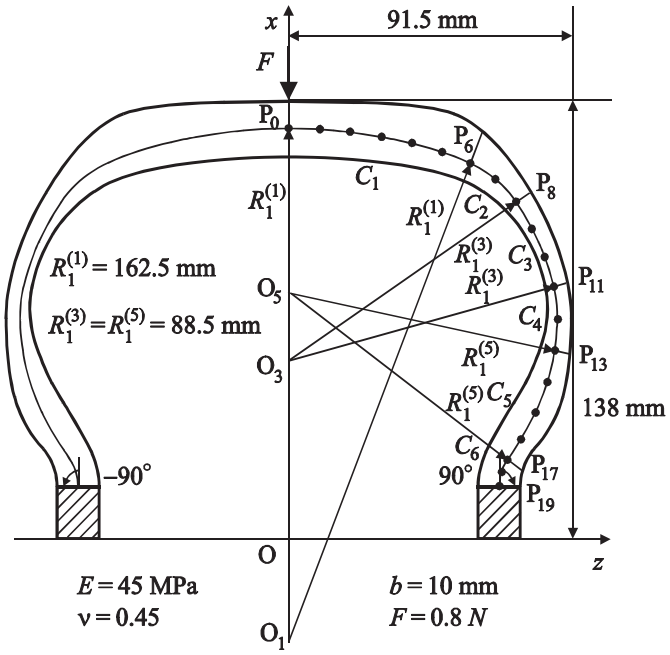

Fig. 22. Polyurethan tire section.

deformed configuration in Fig. 16 and at $f = 1.8$ for all other cases. As in previous examples the GEX4 element leads to a poor prediction of the shell response for very coarse meshes.

6.5. Pinched cross-ply hyperbolic shell

Further we consider a cross-ply hyperbolic shell under two pairs of opposite forces. The geometrical and material data of the three-layer hyperbolic shell are shown in Fig. 19, where 0° and 90° refer to the circumferential and meridional directions.

Due to symmetry of the problem, only one octant of the shell is discretized with uniform meshes. Table 7 and Fig. 20 present displacements derived through using geometrically exact elements for both ply sequences, where u_x^M and u_y^M denote displacements of the midsurface in x and y directions. Fig. 21 displays our results compared with those obtained by Basar et al. [36] and Braun et al. [4] employing the 28 × 28 mesh of bilinear degenerated-shell and 14 × 14 mesh of quadratic solid-shell elements, respectively. One can observe that proposed geometrically exact solid-shell elements perform excellently because only one load step with 8 Newton iterations are needed to derive a converged solution for the [0/90/0] ply orientation with a tolerance of 10^{-8}. Unfortunately, we have no possibility to compare these results with those based on the isoparametric finite element formulation because in papers [4,36] are not mentioned a convergence criterion and load increments.

6.6. Tire section under concentrated load

The last example to be studied is a clamped tire section subjected to a concentrated load at the apex, as depicted in Fig. 22. The polyurethan tire section of width b is assumed to be linearly elastic and homogeneous [37]. One-half of the

Table 8
Tire section geometry

m	0	1	2	3	4	5	6	7	8	9
s (mm)	0.0	10.0	20.0	30.0	40.0	50.0	60.0	70.0	80.0	90.0
x (mm)	129.2	128.8	128.0	126.3	124.3	121.0	118.1	113.2	105.7	97.2
z (mm)	0.0	10.0	19.8	29.7	39.5	49.3	58.2	66.8	73.4	78.2
m	10	11	12	13	14	15	16	17	18	19
s (mm)	100.0	110.0	120.0	130.0	140.0	150.0	160.0	167.8	172.0	177.0
x (mm)	88.6	79.2	69.0	59.1	49.0	39.6	31.2	24.8	21.4	15.3
z (mm)	82.3	85.5	87.0	86.0	83.4	79.7	75.0	71.0	68.7	67.5

Table 9
Transverse displacement (mm) at point P_0 of tire section using 64×1 mesh and residual criterion (51) with tolerance of 10^{-9}

Element	NStep = 1		NStep = 5		NStep = 10	
	$u_3^R(P_0)$	NIter	$u_3^R(P_0)$	NIter	$u_3^R(P_0)$	NIter
GEX4	28.092	5	28.092	16	28.092	31
GEX4A3	28.111	5	28.111	16	28.111	31
GEX4A6	28.148	5	28.148	16	28.148	31

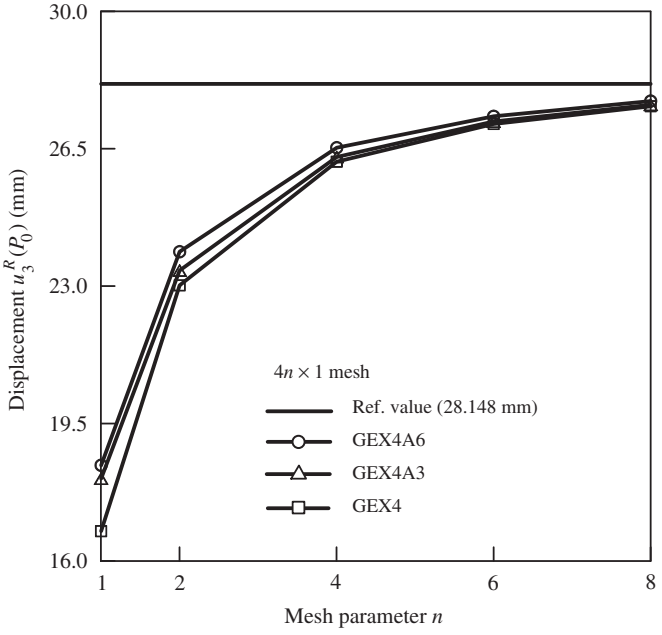

Fig. 23. Convergence study due to mesh refinement for tire section, where reference solution is provided by 64×1 mesh of GEX4A6 elements.

reference tire curve C is composed of six separate curves such that C_1, C_3 and C_5 ones represent the arcs of radii $R_1^{(1)}$, $R_1^{(3)}$ and $R_1^{(5)}$, respectively. The data used to describe tire geometry are listed in Table 8. To apply a numerical algorithm [33], we have taken the mean deviation of the measured coordinate values from their exact ones as 0.3 mm and considered a whole reference curve C, given on a plane by 39 prescribed points, with boundary tangent angles of $\pm 90°$, as shown in Fig. 22.

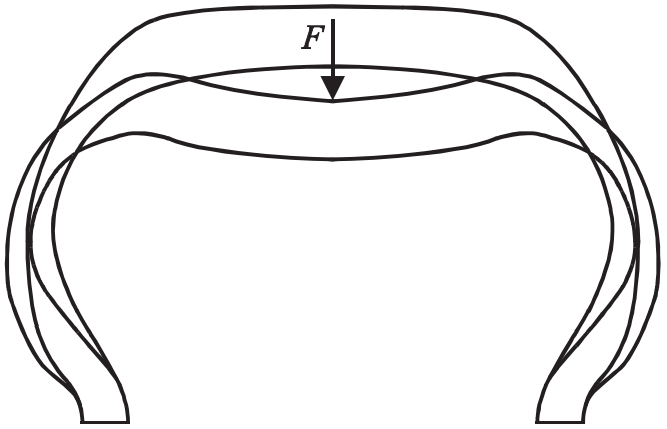

Fig. 24. Deformed tire section.

Owing to symmetry of the problem only half of the tire section is modeled with uniform meshes of geometrically exact elements. Table 9 and Fig. 23 display a transverse displacement of the reference surface u_3^R at point P_0. As a convergence criterion the residual one with $\varepsilon = 10^{-9}$ has been used. It is seen that all results are in a good agreement for all mesh configurations. In addition, Fig. 24 demonstrates a deformed configuration of the tire section.

7. Conclusions

The simple and efficient geometrically exact assumed stress–strain four-node solid-shell elements have been developed for the analysis of multilayered composite shells undergoing finite rotations. The finite element formulation is based on the non-linear strain–displacement relationships written

in curvilinear reference surface coordinates that are invariant under arbitrarily large rigid-body motions. This is due to our approach in which the displacement vectors of the bottom and top surfaces are introduced and resolved in the reference surface frame.

The proposed geometrically exact solid-shell element model is free of assumptions of small displacements, small rotations and small loading steps because it is based on the objective fully non-linear strain–displacement relationships. This model is robust because it allows, first, to use much larger load increments than existing geometrically exact shell elements and, second, to model shell intersections and shell edges of free-form configurations, as in the last numerical example. The analytical description of surface geometry is provided through authors' numerical algorithm of smoothing the data by cubic spline functions.

Three geometrically exact four-node solid-shell elements have been developed. The first element GEX4, based on the conventional assumed stress–strain technique, exhibits locking in the case of coarse meshes. The alternative elements are based on the modified ANS method in which either three or all six components of the natural strain tensor vary bilinearly inside the element, i.e., no expected biquadratic interpolation typical for the non-linear four-node solid-shell elements is employed. In a result the best GEX4A6 element demonstrates an excellent performance for all meshes and extremely large displacements and rotations. It is noteworthy that corresponding element solutions (if they converge) usually yield very close numerical results for fine meshes and all elements developed are *insensitive* to a number of loading steps.

Acknowledgments

The present research was supported by Russian Fund of Basic Research (Grant nos. 04-01-00070 and 07-01-00186). Authors wish to thank the reviewers for their suggestions, which helped to improve this paper.

References

[1] Y.H. Kim, S.W. Lee, A solid element formulation for large deflection analysis of composite shell structures, Comput. Struct. 30 (1988) 269–274.
[2] J.C. Simo, M.S. Rifai, D.D. Fox, On a stress resultant geometrically exact shell model. Part IV. Variable thickness shells with through-the-thickness stretching, Comput. Methods Appl. Mech. Eng. 81 (1990) 91–126.
[3] N. Buchter, E. Ramm, D. Roehl, Three-dimensional extension of nonlinear shell formulation based on the enhanced assumed strain concept, Int. J. Numer. Methods Eng. 37 (1994) 2551–2568.
[4] M. Braun, M. Bischoff, E. Ramm, Nonlinear shell formulations for complete three-dimensional constitutive laws including composites and laminates, Comput. Mech. 15 (1994) 1–18.
[5] H. Parisch, A continuum-based shell theory for non-linear applications, Int. J. Numer. Methods Eng. 38 (1995) 1855–1883.
[6] H.C. Park, C. Cho, S.W. Lee, An efficient assumed strain element model with six dof per node for geometrically nonlinear shells, Int. J. Numer. Methods Eng. 38 (1995) 4101–4122.
[7] P. Betsch, E. Stein, An assumed strain approach avoiding artificial thickness straining for a nonlinear 4-node shell element, Commun. Numer. Methods Eng. 11 (1995) 899–909.
[8] R. Hauptmann, K. Schweizerhof, A systematic development of 'solid-shell' element formulations for linear and non-linear analyses employing only displacement degrees of freedom, Int. J. Numer. Methods Eng. 42 (1998) 49–69.
[9] C. Sansour, F.G. Kollmann, Families of 4-node and 9-node finite elements for a finite deformation shell theory. An assessment of hybrid stress, hybrid strain and enhanced strain elements, Comput. Mech. 24 (2000) 435–447.
[10] K.Y. Sze, W.K. Chan, T.H.H. Pian, An eight-node hybrid-stress solid-shell element for geometric non-linear analysis of elastic shells, Int. J. Numer. Methods Eng. 55 (2002) 853–878.
[11] K.Y. Sze, Three-dimensional continuum finite element models for plate/shell analysis, Prog. Struct. Eng. Mater. 4 (2002) 400–407.
[12] G.M. Kulikov, S.V. Plotnikova, Non-conventional non-linear two-node hybrid stress–strain curved beam elements, Finite Elem. Anal. Des. 40 (2004) 1333–1359.
[13] G.M. Kulikov, S.V. Plotnikova, Finite deformation plate theory and large rigid-body motions, Int. J. Non-Linear Mech. 39 (2004) 1093–1109.
[14] G.M. Kulikov, S.V. Plotnikova, Investigation of locally loaded multilayer shells by a mixed finite-element method. 2. Geometrically nonlinear statement, Mech. Compos. Mater. 38 (2002) 539–546 (translated from Mekhanika Kompozitnykh Materialov 38 (2002) 815–826).
[15] G.M. Kulikov, S.V. Plotnikova, Non-linear strain–displacement equations exactly representing large rigid-body motions. Part I. Timoshenko–Mindlin shell theory, Comput. Methods Appl. Mech. Eng. 192 (2003) 851–875.
[16] G.M. Kulikov, S.V. Plotnikova, Non-linear strain–displacement equations exactly representing large rigid-body motions. Part II. Enhanced finite element technique, Comput. Methods Appl. Mech. Eng. 195 (2006) 2209–2230.
[17] H.Y. Roh, M. Cho, The application of geometrically exact shell elements to B-spline surfaces, Comput. Methods Appl. Mech. Eng. 193 (2004) 2261–2299.
[18] T.J.R. Hughes, J.A. Cottrell, Y. Bazilevs, Isogeometric analysis: CAD, finite elements, NURBS, exact geometry and mesh refinement, Comput. Methods Appl. Mech. Eng. 194 (2005) 4135–4195.
[19] G. Wempner, D. Talaslidis, C.M. Hwang, A simple and efficient approximation of shells via finite quadrilateral elements, J. Appl. Mech. 49 (1982) 115–120.
[20] K.Y. Sze, S. Yi, M.H. Tay, An explicit hybrid stabilized eighteen-node solid element for thin shell analysis, Int. J. Numer. Methods Eng. 40 (1997) 1839–1856.
[21] G.M. Kulikov, S.V. Plotnikova, Equivalent single-layer and layer-wise shell theories and rigid-body motions. Part I. Foundations, Mech. Adv. Mater. Struct. 12 (2005) 275–283.
[22] C. Cho, S.W. Lee, On the assumed strain formulation for geometrically nonlinear analysis, Finite Elem. Anal. Des. 24 (1996) 31–47.
[23] T.J.R. Hughes, T.E. Tezduyar, Finite elements based upon Mindlin plate theory with particular reference to the four-node bilinear isoparametric element, J. Appl. Mech. 48 (1981) 587–596.
[24] R.H. MacNeal, Derivation of element stiffness matrices by assumed strain distributions, Nucl. Eng. Des. 70 (1982) 3–12.
[25] K.J. Bathe, E.N. Dvorkin, A formulation of general shell elements—the use of mixed interpolation of tensorial components, Int. J. Numer. Methods Eng. 22 (1986) 697–722.
[26] K.C. Park, G.M. Stanley, A curved C° shell element based on assumed natural coordinate strains, J. Appl. Mech. 53 (1986) 278–290.
[27] G.M. Kulikov, Analysis of initially stressed multilayered shells, Int. J. Solids Struct. 38 (2001) 4535–4555.
[28] G.M. Kulikov, S.V. Plotnikova, Geometrically exact assumed stress–strain multilayered solid-shell elements based on the 3D analytical integration, Comput. Struct. 84 (2006) 1275–1287.
[29] S.P. Timoshenko, J.N. Goodier, Theory of Elasticity, third ed., McGraw-Hill, New York, 1970.
[30] G.M. Kulikov, S.V. Plotnikova, Assumed stress–strain quadrilateral plate elements based on analytical and numerical integration, Trans. TSTU 12 (2006) 107–121.
[31] A.L. Gol'denveiser, Theory of Elastic Thin Shell, Pergamon Press, Oxford, 1961.

[32] A. Barut, E. Madenci, A. Tessler, Nonlinear analysis of laminates through a Mindlin-type shear deformable shallow shell element, Comput. Methods Appl. Mech. Eng. 143 (1997) 155–173.

[33] E.I. Grigolyuk, G.M. Kulikov, Axisymmetric deformation of anisotropic multilayer shells of revolution of intricate shapes, Mech. Compos. Mater. 17 (1982) 437–445 (translated from Mekhanika Kompozitnykh Materialov 17 (1981) 637–645).

[34] E.I. Grigolyuk, G.M. Kulikov, Multilayered Reinforced Shells: Analysis of Pneumatic Tires, Mashinostroyenie, Moscow, 1988 (in Russian).

[35] Y. Basar, Y. Ding, Finite-rotation elements for the non-linear analysis of thin shell structures, Int. J. Solids Struct. 26 (1990) 83–97.

[36] Y. Basar, Y. Ding, R. Schultz, Refined shear-deformation models for composite laminates with finite rotations, Int. J. Solids Struct. 30 (1993) 2611–2638.

[37] H. Rothert, H. Idelberger, W. Jacobi, G. Laging, On the finite element solution of the three-dimensional tire contact problem, Nucl. Eng. Des. 78 (1984) 363–375.